Detailed Nonlinear Analysis of Bolted Joint

Master's thesis in Applied Mechanics

Deepashri Shrikant Damle

DEPARTMENT OF Industrial and Materials Science

CHALMERS UNIVERSITY OF TECHNOLOGY
Gothenburg, Sweden 2026
www.chalmers.se

Master's thesis 2026

Detailed Nonlinear Analysis of Bolted Joint

DEEPASHRI SHRIKANT DAMLE

CHALMERS
UNIVERSITY OF TECHNOLOGY

Department of Industrial and Materials Science
Division of Material and Computational Mechanics
Chalmers University of Technology
Gothenburg, Sweden 2026

Detailed Nonlinear Analysis of Bolted Joints.
DEEPASHRI SHRIKANT DAMLE

Supervisor: Lisa Kilsmark, Department of CAE and Vehicle Safety, AFRY AB, Trollhättan
Examiner: Fredrik Larsson, Department of Industrial and Materials Science

Master's Thesis 2026
Department of Industrial and Materials Science
Division of Material and Computational Mechanics
Chalmers University of Technology
SE-412 96 Gothenburg
Telephone +46 31 772 1000

Typeset in LaTeX
Printed by Chalmers Reproservice
Gothenburg, Sweden 2026

Detailed Non-linear Analysis of Bolted Joint
DEEPASHRI SHRIKANT DAMLE
Department of Industrial and Materials Science
Chalmers University of Technology

Abstract

Bolted joints are widely used in industrial applications due to their strength and ease of assembly. The most important characteristic of a bolted joint is its ability to prevent sliding motion between the joint parts when subjected to vibrations as well as external loading, by exerting a compressive force on the joint members. The clamping force generated during the assembly process is a function of various factors like the applied torque, material of the joint, behaviour of contact interfaces, as well as external conditions such as temperature. This project aims to understand the behaviour of a bolted joint during the assembly process with an applied torque. The finite element method is used to analyse the interaction between different components of a bolted assembly during its tightening process. A detailed 3D model is implemented in the finite element software ABAQUS. Torque is applied and then removed to simulate the tightening and torque tool removal. How friction affects this process is studied by varying the friction coefficient at the under-head interface. Results obtained from finite element analysis show agreement with commonly used handbook calculations for bolted joints. Varying under-head friction shows that the bolt preload does not drop significantly during torque removal; however, the friction under the head is found to affect the rate of preload drop after assembly. The analysis presented in this study can be further adapted to study the effect of other factors, like material properties, loading rate during tightening, as well as the response under external loads.

Keywords: Bolted joint, FE analysis, tightening process, friction, torque control.

Acknowledgements

I would like to thank all contributors and stakeholders for their valuable contributions towards the completion of this thesis. I would also like to thank my supaervisor, Lisa Kilsmark from AFRY AB for her constant guidance and support throughout the project. I am also grateful to the Department of CAE and Vehicle Safety, AFRY AB, Trollhättan for providing the opportunity, guidance and tools for completing this thesis. Finally, I would like to thank my examiner, Fredrik Larsson at Chalmers University of Technology for his support.

Deepashri Damle, Gothenburg, June 2026

Nomenclature

Below is the nomenclature of variables that have been used throughout this thesis.

Variables

$\mu_{underhead}$	Friction coefficient at the bolt-clamped part interface
μ_{thread}	Friction coefficient at the internal and external threads interface
$T_{applied}$	Applied torque at the bolt head
$T_{underhead}$	Contact friction torque at the bolt-clamped part interface
T_{thread}	Contact friction torque at the internal and external threads interface
T_{pitch}	Portion of the applied torque that converts to preload
$F_{preload}$	Preload generated in the bolt
D_{km}	Equivalent diameter for torque calculation at the bolt-clamped part interface
d_m	Thread pitch diameter
p	Thread pitch
u_x, u_y, u_z	Displacements in x, y, z directions, respectively

Contents

List of Acronyms ix

Nomenclature ix

List of Figures xiii

List of Tables xv

1 Introduction 1
- 1.1 Background . . . 1
  - 1.1.1 Bolted Joint under External Loads . . . 1
  - 1.1.2 Bolt Preload . . . 2
- 1.2 Literature Review . . . 3
  - 1.2.1 Applied Torque - Bolt Preload Relationship . . . 3
  - 1.2.2 Bearing Surface Friction . . . 4
  - 1.2.3 Thread Friction . . . 4
  - 1.2.4 Tightening Process of a Bolted Joint . . . 5
  - 1.2.5 Preload Variation after Assembly . . . 5
- 1.3 Purpose and Aim . . . 6
- 1.4 Problem Description . . . 7
- 1.5 Scope and Limitations . . . 8

2 Analysis Process 11
- 2.1 Preload Generation Process . . . 11
- 2.2 Finite Element Analysis Process . . . 12
  - 2.2.1 Bearing Surface Friction Variation . . . 13

3 Methods 15
- 3.1 Baseline Finite Element Model and Analysis . . . 15
  - 3.1.1 Mesh . . . 15
    - 3.1.1.1 Bolt and Threaded part . . . 16
    - 3.1.1.2 Clamped part . . . 17
    - 3.1.1.3 Couplings and Springs . . . 18
  - 3.1.2 Material . . . 20
  - 3.1.3 Contact Conditions . . . 20
  - 3.1.4 Boundary Conditions . . . 21
  - 3.1.5 Analysis Procedure . . . 22

3.2 Hand Calculations 24
3.3 Under-head Friction Variation 25

4 Results **27**
4.1 Baseline model 27
4.1.1 Bolt - Clamped part Contact 27
4.1.2 Thread Contact 28
4.1.3 Clamped part - Threaded part Contact 29
4.1.4 Axial and Torsional Displacement Results 30
4.1.5 Torque Evolution Through Time 32
4.1.6 Preload Evolution Through Time 33
4.1.7 Agreement between Hand Calculation and FE Results 33
4.1.8 Equivalent Stress Results 34
4.2 Effect of Under-head Friction 35
4.3 Sources of Error 37

5 Conclusion **39**
5.1 Scope for future work 40

Bibliography **41**

List of Figures

1.1 Forces in a bolted joint under tensile external load 2
1.2 Forces in a bolted joint under shear external load 2
1.3 Assembly: From above 7
1.4 Assembly: From below 7
1.5 Assembly: Section through bolt axis 8
1.6 Illustration of how different quantities analysed in this study act on the bolt 9

3.1 Threaded part: Different mesh regions 16
3.2 Bolt: Different mesh regions 16
3.3 Clamped part: Mesh 18
3.4 Springs on the bolt 19
3.5 Distributing couplings defined at different sections on the bolt 19
3.6 Clamped part - top surface couplings 19
3.7 Clamped part - bottom surface couplings 19
3.8 Different contact regions in the model 20
3.9 Boundary conditions on the clamped part and threaded part 22
3.10 Boundary conditions on the bolt 22
3.11 Gaps between the contact surfaces 23
3.12 Rotation amplitude curve 24
3.13 Torque amplitude curve 24

4.1 Under-head contact pressure distribution at 90 Nm 27
4.2 Average under-head contact pressure at 90 Nm 27
4.3 Bolt thread numbers 28
4.4 Variation in contact pressure at different points along the bolt at 90 Nm 28
4.5 Radial locations of nodes on the thread surface 28
4.6 Average contact pressure at different threads at 90 Nm 28
4.7 Contact pressure distribution at 90 Nm 29
4.8 Different contact surfaces at the clamped part - threaded part contact interface 29
4.9 Contact pressure distribution at the clamped part - threaded part interface 29
4.10 Points at different sections of the bolt 30
4.11 Relative axial displacement of points at different sections along the bolt axis 30

4.12 Relative rotational displacement of points at different sections along the bolt axis . . . 31
4.13 Axial force and deformation in the bolt and the clamped part . . . 31
4.14 Variation of different torque components through the analysis . . . 32
4.15 Bolt preload variation through analysis . . . 33
4.16 Bolt: Von Mises stress . . . 34
4.17 Bolt: Von Mises stress - section view . . . 34
4.18 Clamped part: Von Mises stress - from top . . . 34
4.19 Clamped part: Von Mises stress - from bottom . . . 34
4.20 Threaded part: Von Mises stress - from top . . . 35
4.21 Threaded part: Von Mises stress - from bottom . . . 35
4.22 Preload drop . . . 35
4.23 Shank torque drop . . . 35
4.24 Reduction in twist of the bolt shank . . . 36
4.25 Case 1: $\mu_{underhead} = 0.07$ . . . 36
4.26 Case 2: $\mu_{underhead} = 0.08$ . . . 36
4.27 Case 3: $\mu_{underhead} = 0.12$ . . . 37

List of Tables

3.1 Mesh overview 15
3.2 Mesh parameters for the bolt and the threaded part 17
3.3 Shell mesh quality criteria for clamped part 17
3.4 Solid mesh quality criteria for clamped part 17
3.5 Materials for different parts 20
3.6 Different contact regions in the assembly 20
3.7 Friction coefficients at different assembly interfaces 21
3.8 Summary of analysis steps 23
3.9 Baseline model - hand calculation data 24
3.10 Hand calculation results for different under-head friction coefficients tested 26

4.1 Comparison of hand calculation and FE results 34

1
Introduction

This chapter discusses the background and motivation of this study. Previous work on the topic has been presented in brief through a literature review section. The aim and objectives of the project are then specified. The bolted joint under consideration in the project is presented. Finally, scope of the analysis is described.

1.1 Background

Bolted joints are widely used in industrial applications due to their strength and ease of assembly. The most important characteristic of a bolted joint is its ability to prevent sliding motion between the joint parts due to vibrations, as well as other types of external loads and ensure structural integrity of the assembly. By applying a torque, an axial (tensile) force is generated in the bolt as a reaction of clamping the assembled parts together. To ensure the integrity of the assembly, it is necessary to maintain a certain level of contact pressure between the clamped parts. The relationship between torque and generated clamping force depends on the frictional properties of the assembly interfaces, material characteristics of all the materials involved in the joint, as well as the magnitude of applied torque [1].

1.1.1 Bolted Joint under External Loads

The bolted joint can be loaded in axial as well as shear directions. The path of load transfer between parts of the joint when the joint is loaded axially or in shear is different. With an axial external load, the load transfer occurs mainly by bearing stresses on the surfaces in contact. If tensile loads are applied to the assembly, sufficient compressive (contact) forces should be present between the joint parts in order to maintain the integrity of the assembly. Insufficient contact forces can lead to failure by either plastic deformation of the threads, or tensile failure under the bolt head.

Under shear loading, the load transfer path depends on the magnitude of external load applied. However, the purpose of the joint in this case is to prevent relative slipping between the joint parts. Thus, when the applied external load exceeds the critical shear load for the joint, bearing stresses are generated in the bolt, and the load transfer mechanism changes from frictional slipping to bearing. This can lead to the joint failure by shear failure of the bolt. The critical shear load depends on

the contact pressure between the joint parts, and the friction coefficient. Thus, it is important to maintain sufficient contact pressure in the assembly throughout the operational life of the joint.[2]. The different load paths in a bolted joint under different types of external loads are illustrated in figures 1.1 and 1.2.

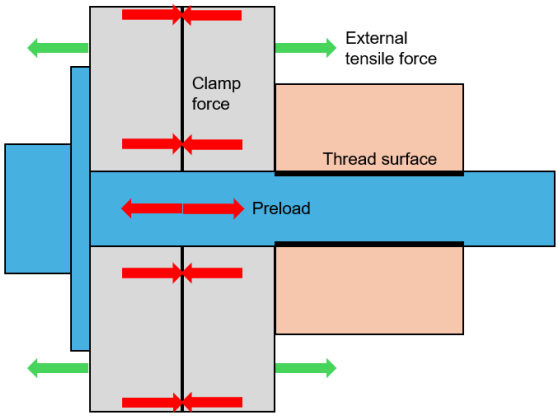

Figure 1.1: Forces in a bolted joint under tensile external load

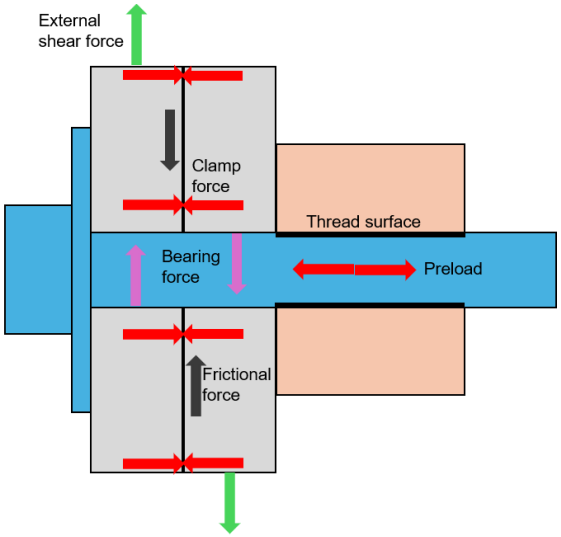

Figure 1.2: Forces in a bolted joint under shear external load

1.1.2 Bolt Preload

Compressive force on the joint parts is generated by applying a torque on the bolted joint. When the bolt is tightened, the nut exerts a contact force on the assembled parts which results in their compression, and experiences a reaction from the assembled parts. This reaction force points outwards from the joint, and is transferred from the nut to the bolt through the threads. This results in tensile stresses generated in the bolt, and compression of the assembly. This force is called bolt 'preload' or 'pretension', and it is important to maintain the preload to the designed level throughout the operational life of the joint.

Many analytical models have been developed to estimate the preload generated for a given applied torque or force as described in [1], however, the complexity of the actual preload generation process is not captured through simplified analytical models.

The relationship between applied torque on the bolt and the generated preload can be described by a 'nut factor' for simplicity. This gives a linear relationship between applied torque and generated preload. The equation for this preload-torque relationship is given by $T = P\,D\,K$. Here, T is the applied torque, P is bolt preload, D is the nominal diameter of the bolt, and K is the nut factor. This nut factor has a constant value and it encompasses all the factors that affect this torque-preload relationship. The nut factor cannot be determined through analytical equations and needs to be estimated through physical testing. The laboratory conditions under

which the nut factor is measured are hardly found at the actual application of the joint, making the estimation of preload using nut factor unreliable.

Elastic relaxation of the bolt after assembly affects the final, usable preload on the bolt. The bolt relaxation behaviour is complex. However, two distinct regions are found in the relaxation behaviour of the bolt. In the first part of the relaxation curve, the preload loss is rapid. This phase is called as 'short term relaxation' and the behaviour of the joint is also almost linear in this region. However, after a certain amount of time, the slope of the relaxation curve changes and the preload drop becomes much more gradual. This phase is called as 'long term relaxation'. Further, this part of the relaxation curve is also dependent on the time passed. The preload drops at a low rate, and the duration of the analysis will affect the results. While long term relaxation is a complex phenomenon, the preload drop during this phase is much less compared to the 'short term relaxation phase' [2].

Direct measurement of bolt preload cannot be done. A number of techniques like measurement of bolt strain, measurement of torque required to open the joint completely, measurement of torque required to re-tighten the joint after a certain time following the initial assembly exist, which can give an indirect measurement of preload with varying levels of accuracy and cost.

Due to the complex nature of the relationship between specified torque and preload outcome, it is difficult to construct a safe bolted joint from a tightening perspective. Thus, it is essential to properly quantify the working preload for a given applied torque for critical applications.

1.2 Literature Review

1.2.1 Applied Torque - Bolt Preload Relationship

The relationship between applied torque and generated preload in the bolt has been studied extensively over many years. Many analytical models have been developed to calculate the preload generated in a bolt for a given value of the applied torque. The 'long-form torque-preload' equation $T_{applied} = T_{underhead} + T_{thread} + T_{pitch}$ in [2] divides the applied torque into three portions - torque consumed to overcome the friction at the bearing surface, torque consumed to overcome the friction at the thread surface, and the remaining torque that is actually utilised to create the preload in the bolt, i.e. T_{pitch}. Each of these portions are defined as a function of the preload developed in the bolt. Friction coefficients at the bearing and thread interfaces are taken into account in this equation. This equation is widely used to estimate the generated preload in the bolt, when no plastic deformation is expected in the bolt.

As the geometry of the bolt is highly irregular, the stresses generated in the bolt threads are much higher than those in the bolt shank. Thus, the bolt threads are at a much higher risk of yielding than the bolt shank. It is recommended in the literature

that the maximum preload generated in the bolt should not be more than 70% of the tensile force required to induce yielding in the bolt. There are many simplifications made in the analytical models developed for calculating the preload generated in the bolt. The effect of stress concentration at the threads, effect of plastic deformation of the surface roughness during tightening process, effect of non-uniform contact pressure distributions, effect of changing friction coefficients has not been considered in the analytical models. These factors have been studied individually in several studies.

1.2.2 Bearing Surface Friction

The torque required to overcome the bearing friction depends on factors like contact pressure between the contacting bodies, the friction coefficient at the interface, as well as the equivalent friction radius. It is the distance between the bolt axis and the location of the equivalent normal force acting on the contact surface. The effect of these factors on the torque consumed due to friction at the bearing surface has been studied in [3, 4, 5].

In the long-form equation from [2], it is assumed that the contact pressure is uniform all over the bearing surface area. However, in reality the pressure is higher near the bolt shank, and decreases as the distance from the bolt axis increases. The effect of different contact pressure distributions on the equivalent friction radius of the bearing surface has been studied in [3]. It has been found that using the mean radius of the active contact as equivalent friction radius for bearing friction torque calculation is more erroneous for higher values of the ratio of outer radius of the contact surface to the inner radius of the contact surface. The effect of varying sliding speed on the bearing surface friction coefficient is also studied and it is also found to be more pronounced for higher values of the ratio of the outer to the inner bearing surface radius. The under-head contact pressure distribution is modelled by considering a punch problem in [4], and another expression of equivalent friction radius is obtained. With proposed equivalent friction radius expressions, the results are found to be well in agreement with the experiments conducted, however a comparison with the results using mean radius is not made.

1.2.3 Thread Friction

A major component in the torque-preload relationship is the torque consumed by friction at the threads. It also depends on the contact pressure, the friction coefficient, and the distance from the bolt axis. In the long-form equation from [2], a constant friction coefficient is assumed, along with the thread mean radius as equivalent friction radius for thread friction torque calculation. The effect of different pressure distributions on the equivalent friction radius for torque calculation is studied in [6], and it has been concluded that for the range of ratio of thread major diameter to thread minor diameter commonly found in the commercially used bolts,

it is sufficiently accurate to use the mean thread radius as the equivalent friction radius for thread friction torque calculation. In reality, the contact pressure is found to be higher at the tip of the bolt thread, and lower at the roots. However, it is important to note that the friction coefficient does not remain constant in reality, as the thread surface undergoes wear and plastic deformation [5]. Effect of lubrication on the bearing and thread surface is analysed experimentally with repeated tightening tests in [7], where lubrication is found reduce the variability in the generated preload after repeated tightening tests.

1.2.4 Tightening Process of a Bolted Joint

The tightening process of the bolt using various methods has been studied many times in the literature with simulation, experiments, and using analytical models [8, 9, 10, 11, 7]. Different methods for tightening the bolt, e.g. torque control[9, 11, 7] and use of hydraulic tensioners[8] has also been studied. Earlier axisymmetric finite element models have been used to simulate the tightening process of a bolted joint [8]. The elastic - plastic behaviour of a bolted joint is studied through a 3D finite element analysis with 2D elements, i.e. 3 degrees of freedom per node in [9]. A higher value of thread friction was found to decrease the threshold for non-linear relationship between the axial stress generated in the bolt (a measure of bolt preload) and the axial deformation caused due to the applied torque. This behaviour agrees well with the established material behaviour in general. The authors also state that larger value of the bearing friction coefficient causes a higher portion of the contact zones to develop plastic deformation. From [10], thread friction is also found to be affecting the load distribution between the threads.

The bolt preload also depends on the stiffness of the joint. A stiffer bolt will store more elastic strain energy than a soft bolt for the same deformation. However, plastic deformation causes significant decrease in the generated preload, as stiffness of the bolt reduces significantly with plasticity [9]. Ratio of elastic moduli of bolt and clamped parts has been tested to see it's effect on the torque - preload relationship, however little effect is found in the elastic region[11].

1.2.5 Preload Variation after Assembly

After a bolted joint is tightened and the tightening tool is removed, the stresses in the components stabilise, the parts settle into each other, and load is redistributed in the joint. This load redistribution may lead to some displacement of the components after the tightening process is complete, resulting in preload loss. There are many causes for this preload loss after assembly, like material creep, elastic spring-back, contact creep, etc. This loss in preload can be categorised into two parts - one initial part where the preload drops quite fast after the torque application is complete, and one part where the preload-time curve has a much lower slope and the preload drops at a much lower rate [2].

The initial preload loss is in a bolt after assembly is measured experimentally, and the effect of the factors affecting this preload loss such as friction coefficients and the value of the generated preload during tightening process is analysed in [7]. Effect of the friction coefficients at the contact interfaces, and the effect of initial preload on the self loosening is investigated in [12] under both elastic and elastic-plastic conditions through a three dimensional finite element analysis. Causes for the initial preload drop are hypothesised and tested through the finite element analysis, and the primary cause for the preload drop under no external load is found to be the elastic-plastic deformation of the bolt and the slipping of the threads due to elastic spring-back of the bolt shank also affects the drop in the preload. Bearing surface friction is found to be the only preventing factor for self-loosening of joints after assembly [13].

There is a general agreement among all the studies considered here, that lowering the friction coefficients would generate more "initial" preload [2, 9, 11]. Lowering friction by lubricating the joint reduces scatter in the generated preload and improves the repeatability[4, 14]. However, a lower friction coefficient also reduces the resistance to self loosening behaviour, causing preload loss due to bolt relaxation. From the literature survey, it can be concluded that friction at different assembly interfaces affects the bolt preload significantly both during the tightening process as well as after assembly. In the surveyed literature, independent analysis of effect of friction at different assembly surfaces on the bolted joint response through finite element method is not found. In this project this effect is studied.

1.3 Purpose and Aim

In order to estimate the working preload in a bolted joint, the factors that affect torque-preload relationship during the tightening process need to be analysed. Factors such as surface friction, material properties, applied torque all affect the generated preload during tightening, as well as preload loss after assembly.

Accurate analysis of such factors through analytical models is difficult, and experimental analysis requires precise control of the environment and control factors. Further, the variability in the manufactured parts increases the level of uncertainty in the results obtained from experiments. Finite element method gives a faster and economical way to analyse a bolted joint than physical tests. It also allows analysis of different parameters through the same model.

From the literature survey, friction is found to be affecting many phenomena that alter the generated preload in the bolt. By only varying frictional properties, the torque-preload relationship can be altered significantly. In this study, the effect of bearing surface friction on the joint's response is studied through finite element analysis.

The specific objectives of the project can be listed as follows:

1. Establish the relationship between the generated preload and applied torque in a bolted joint through finite element simulation of the tightening process with set applied torque.

2. Study the effect of bearing surface friction on the behaviour of the joint in terms of bolt preload, torque in the bolt, and twist in the bolt.

1.4 Problem Description

The bolted joint under consideration in this study consists of a M12 × 1.75 bolt, a clamped part, and a threaded part. The meshed model of the assembly is shown in figures 1.3, 1.4, 1.5.

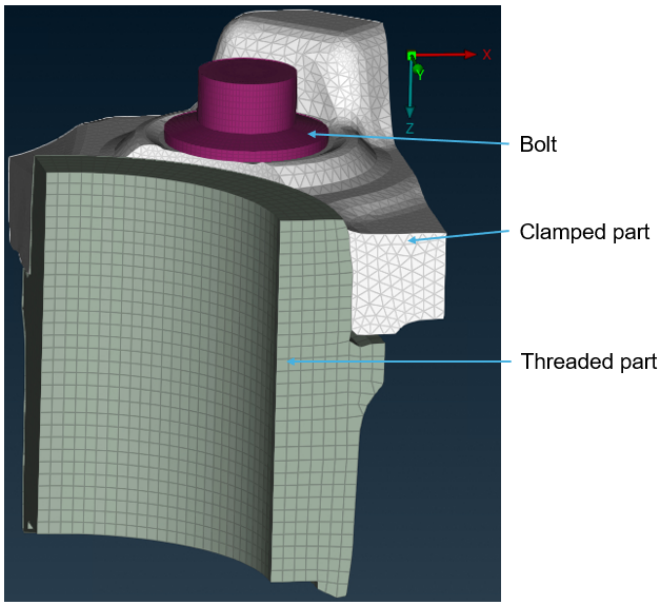

Figure 1.3: Assembly: From above

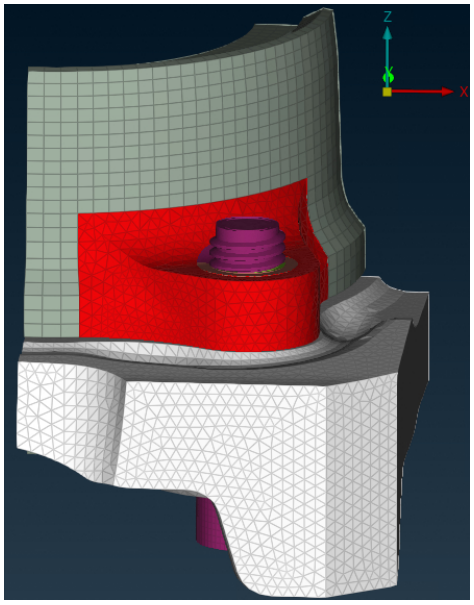

Figure 1.4: Assembly: From below

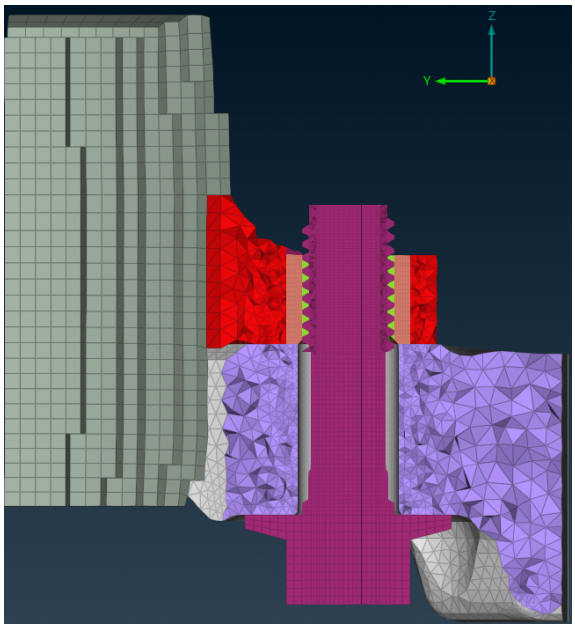

Figure 1.5: Assembly: Section through bolt axis

Physical tightening tests have been performed on the joint to measure the resulting preload and torque in the bolt shank. The bolt is thus modified to mount the measuring instruments. This includes reduction in the diameter of the bolt shank, which is also represented in the finite element model. Response of the joint under a tightening torque of 90 Nm applied on the bolt is studied in this project.

1.5 Scope and Limitations

In this study, the goal is to analyse the effect of bearing surface friction on the tightening process of the bolted assembly described in Section 1.4. In the assembly under consideration, the bearing surface is the contact surface under the bolt head. The analysis is run with a set value of applied torque on the bolt, and the response of the joint is evaluated in terms of the preload generated in the bolt, torque in the bolt, as well as axial and torsional deformation in the bolt. Additionally, the equivalent stress results in all the components are checked to ensure that none of the components undergo any plastic deformation under the prescribed loads. For verification of results from the finite element analysis, handbook calculations as well as the experimental results are used. Quantitatively, the results are thus relevant only for the joint considered in the study. The metrics related to the bolted joint whose variation will be studied in the project are shown in Figure 1.6.

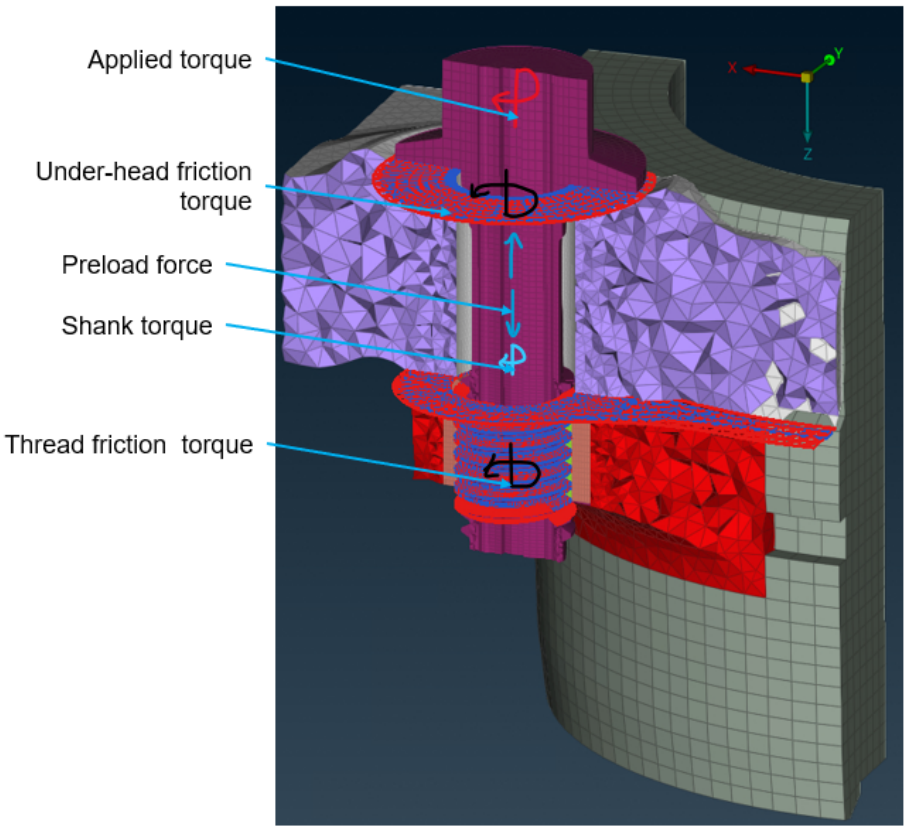

Figure 1.6: Illustration of how different quantities analysed in this study act on the bolt

Appropriate description of different contact surfaces is crucial for accurate results. This entails defining different friction properties for different contact surfaces based on the underlying materials of the contacting bodies. While it has been found through literature study that frictional properties themselves change during the tightening process, in this study only the effect of different conditions of friction is considered.

Additionally, the material model should be able to capture the stress response under the specified loads accurately. Results from the physical tests performed on the joint do not show any plastic deformation in the bolt under the prescribed applied loads. Since the same load value as experiments is used in the finite element analysis, linear elastic material model is used for all the joint parts in the finite element analysis.

Bolt tightening is a complex process to capture with finite element analysis. To simplify the analysis, certain limitations are put on the study, as follows:

1. **Mesh sensitivity studies**
   The results are not checked for mesh convergence as the analysis takes significant time to converge. Handbook calculations and experimental results are used to verify the analysis results.

2. **Dynamic effects**
   The analysis is run in quasi-static conditions for simplicity, and dynamic effects such as effect of different speeds of load application will be neglected.

3. **Coefficient of friction**
   Coulomb friction model is used at the contact interfaces in the assembly, and variation of friction due to phenomena such as wear and embedding is not considered. Additionally, variation of friction coefficient based on relative sliding speed or contact pressure is also excluded from this project.

2

Analysis Process

This chapter discusses the process of the analysis. A brief description of how preload is generated in a general bolted assembly is given, and some terms related to the tightening process are explained. This is followed by a description of how the finite element model in this study captures this behaviour.

2.1 Preload Generation Process

When a bolt or nut is tightened, initially, the applied torque only needs to overcome friction at the threads in order to give rotational movement of the bolt or nut. However, when the bolt head or nut comes into contact with the joint, the joint resists the axial movement of the bolt or nut. This contact surface is called as bearing surface. When the bolt or nut is further rotated in this state, friction at this bearing surface resists the rotational motion, and the normal force resists the axial movement. Thus, now the torque applied on the bolt or nut must overcome friction at both the thread surface, as well as the bearing surface for any movement. In this process, the bolt experiences both tensile and shear stresses. The bolt preload corresponds to these tensile stresses, and the torque in the bolt shank corresponds to these shear stresses.

Frictional resistance offered by the different contact interfaces during tightening process depends on the normal forces. When torque is applied on the bolt or the nut after contact with the bearing surface, it results in an increase in normal force at the bearing surface and thread surface as the bolt or nut exerts more and more pressure on the bearing surface due to its movement. This results in an increase in the resisting frictional torques at these surfaces as well. Bolt or nut movement occurs only if the applied torque is more than the frictional resistance torques on these surfaces. However, with movement, the normal forces as well as the frictional forces increase.

At the threads, the normal force at the contact interface is not perpendicular to the bolt axis, and it also exerts a torque on the bolt along the bolt axis direction. This torque corresponds to the preload generated in the bolt, and is called as pitch torque. During tightening operation, there is equilibrium between the external applied torque, frictional resistance torques and pitch torque.

When the torque tool is removed, the external load which has induced normal and shear stresses in the bolt disappears instantaneously. This results in an imbalance between the external and internal forces and moments in the bolt, causing the generated stresses to reduce due to material elasticity. In the case of a bolt, such stress reduction is primarily in the form of relaxation of internal shear stresses, as the torque is removed, and the threads lock the movement of the bolt in axial direction. This effect is referred to as elastic spring-back. Due to the decrease in the shear stresses, the torque at different sections of the bolt also reduces. This change in torque causes back rotation of the bolt if the friction at the contact interfaces is not enough.

The frictional torques at different contact interfaces also change in direction when torque tool is removed. If the torque imbalance created by removal of external torque is more than the resisting frictional torque at all of the contact interfaces, the joint undergoes loosening. This also results in a drop of contact pressure at these interfaces, and a drop in preload.

When the bolt is under tensile stress for a long time, it undergoes permanent deformation through material creep. This creep is governed by viscoplastic material behaviour. This results in permanent deformation of the bolt under sustained load, which results in the loss of bolt preload.

2.2 Finite Element Analysis Process

When torque is applied on the bolt in a finite element model, it translates to shear stresses in the bolt. The bolt elements act as torsional springs attached to each other and store the applied torque in the form of strain energy in these springs, as long as the material behaviour is linear elastic. At the same time, if the contact is closed at all the contact interfaces, there will be frictional resistance to the movement of the bolt, proportional to the normal force between the contacting surfaces. If the applied torque magnitude in this case is less than the frictional resistance torque, this would result in torque transmission at the contact interfaces, which would induce twist in the components of the assembly. This can be considered as 'sticking' state of contact. When the applied torque is increased beyond the frictional resistance torques at the different contact surfaces, it causes rotation of the bolt. In this case, the contact state is 'slipping'. Preload is generated in the bolt when the contact state is 'slipping'.

Thus, it is important to have minimum possible value of contact pressure before the start of the torque application process, so that contact status can be 'slipping' from the start of the analysis and preload increases from the start. This state is ensured by just closing any contact gaps in the model before start of torque application.

During torque application, stretching of the bolt and compression of the joint occur simultaneously. For compression of the joint, both surfaces of the joint shout be in

contact with the threaded members, i.e. the bolt and the threaded part in this case. To simulate the real process, this contact should be caused by the movement of the bolt through the threaded part. In the finite element model, this behaviour is added by not restricting the movement of the clamped part in the direction of the bolt axis. Thus, the clamp is formed with bolt movement under torque application. To study how preload changes with applied torque, it is applied gradually. The applied torque variation in the finite element analysis is linear.

From experimental results, the bolt preload drop after assembly shows two distinct phases. In the first phase, the preload drops linearly at a high rate, and the rate of preload drop changes after some time. This initial preload drop is captured through removal of applied torque. The elastic spring-back of the bolt is simulated by gradually reducing the applied torque. In this study, linear torque decrease is applied.

2.2.1 Bearing Surface Friction Variation

As concluded from the literature study, frictional behaviour influences the preload variation in the bolt in many ways. The main objective of this friction sensitivity study is to identify how friction at the under-head interface affects the bolt movement during torque release. Thus, determination of values of friction coefficient to test is also affected by the relations between the shank torque and the friction torques at the under-head and thread interfaces.

Bolt head movement during torque removal process depends on the friction coefficient under the bolt head, as described in Section 2.1. For the bolt head to move in the reverse direction when the torque is reduced, the torque at the under-head section of the bolt should be higher than the under-head friction torque. When the applied torque is reduced, the section torques at different sections of the bolt will also drop in magnitude. The maximum value of $T_{underhead}$ is at full torque level (90 Nm applied torque). Thus, when the applied torque is reduced, $T_{underhead}$ changes by a small amount in the opposite direction. When the change in section torque under the bolt head is higher in magnitude than the change in $T_{underhead}$, the bolt head moves. This movement continues until all of the applied torque is released. To simulate different conditions of elastic spring-back and slip under the bolt head during torque removal process, the value of friction coefficient is varied such that a certain ratio is maintained between the shank torque and applied torque in the bolt. This process is described in Section 3.3.

3
Methods

In this chapter, first the baseline finite element analysis setup is described through mesh, materials, contact definitions, boundary conditions and analysis procedure. Further, the procedure followed for estimating the values of frictional torque components and the preload force through hand calculations is presented. Finally, the procedure followed for varying the under-head friction is described.

3.1 Baseline Finite Element Model and Analysis

This section describes the analysis set up to obtain the relationship between torque and preload generated in a bolt with the finite element method. The model is explained through mesh, contact definitions, materials, boundary conditions and load steps.

3.1.1 Mesh

A 3D finite element model for the bolt, clamped part, and threaded part is used for the analysis. Different types of elements are used for different parts based on the geometry, stiffness required, and the discretisation required for different contact interfaces. A detailed description of the mesh in different parts of the model is given in sections 3.1.1.1 and 3.1.1.2. Table 3.1 gives a brief overview of the number and type of elements and the number of nodes in each part of the assembly.

Table 3.1: Mesh overview

Part	Number of elements	Number of nodes	Hex elements	Tet elements
Bolt	137967	195422	53671	84296
Clamped part	78678	101204	0	78678
Threaded part	73934	106023	28712	45222
Total	**290579**	**402649**	**82383**	**208196**

Including the elements and nodes created by the couplings and the springs as described in Section 3.1.1.3, the total number of nodes in the model is **402671** and the total number of elements is **290584**.

3.1.1.1 Bolt and Threaded part

Geometry of the threaded part is highly irregular. Further, much smaller elements are required in the threads than in the bulk of the part. Different types of elements are used in different regions of the threaded part. The threaded part has five mesh regions as shown in Figure 3.1. These different regions are connected by TIE constraints at the interfaces. There are TIE constraints at interfaces between the parts Central cylinder - flange, fillet - threads cylinder, threads cylinder - flange. The nodes on the two surfaces are aligning so that the deformation field across the barrier is smooth.

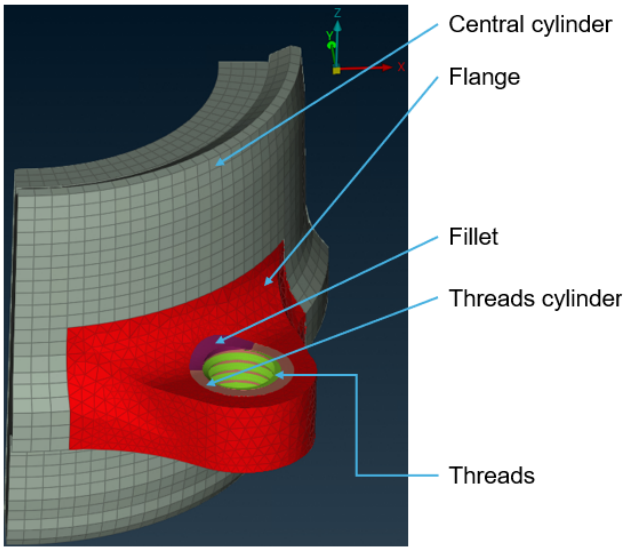

Figure 3.1: Threaded part: Different mesh regions

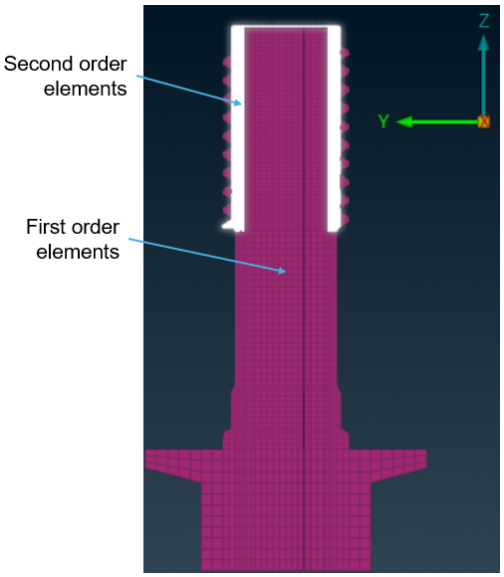

Figure 3.2: Bolt: Different mesh regions

The bolt also consists of different types of elements, as the element size required at the threads is much smaller than the rest of the bolt. For efficiency, only the threads are meshed with smaller elements. To connect the smaller thread elements to the larger shank elements, there is a layer of 2^{nd} order tetrahedral elements in between. Different elements in the bolt are shown in Figure 3.2.The threads on both the bolt and the threaded part are modelled with first order elements. The element size in the threads is ≈ 0.3mm. Table 3.2 shows the mesh parameters for different regions in the bolt and the threaded part.

Table 3.2: Mesh parameters for the bolt and the threaded part

Part	Element type	Element size [mm]	Number of elements	Total
Bolt	8-node Hex	∼0.3 - 1	53671	**137967**
	10-node Tet	∼0.3-0.4	84296	
Threaded part - Central cylinder	8-node Hex	∼2	5594	
Threaded part - Flange	10-node Tet	∼0.4-2.6	41362	
Threaded part - Thread cylinder	8-node Hex	∼0.3-0.6	18551	**73974**
Threaded part - Fillet	10-node Tet	∼0.3-0.45	3860	
Threaded part - Threads	8-node Hex	0.3	4607	

3.1.1.2 Clamped part

The geometry of the clamped part is difficult to capture with a structured hexahedral mesh. The internal response of the clamped part is of little importance in this study, thus it is meshed with an unstructured 2nd order tetrahedral mesh. The geometry was first meshed with 2 mm shell elements and then the volume was meshed with tetrahedral elements. All the elements were then converted to second-order elements. The mesh quality parameters used for the shell mesh and solid mesh are given in tables 3.3, 3.4.

Table 3.3: Shell mesh quality criteria for clamped part

Criterion	Value
Aspect ratio	4
Jacobian	0.8
Min. length [mm]	0.2
Max. length [mm]	7
Min. angle quads [deg.]	45
Min. angle trias [deg.]	135
Min. angle [deg.]	20
Max. angle [deg.]	120
Mid-point deviation [%]	10
Mid-point alignment [%]	33

Table 3.4: Solid mesh quality criteria for clamped part

Criterion	Value
Aspect ratio	8
Jacobian	0.7
Min. length [mm]	0.2
Max. length [mm]	7
Min. angle tetras [deg.]	20
Max. angle tetras [deg.]	120
Min. angle pentas [deg.]	30
Max. angle pentas [deg.]	120
Min. angle hexas [deg.]	30
Max. angle hexas [deg.]	140

The clamped part has contact interface with the bolt head. Thus, the element size on the contact surface is kept comparable to the element size on the bolt head by defining "washer zones" in the mesh parameters for the shell mesh of the clamped part. In total 6 concentric rings are created around the bolt hole, with approximate element size of 1 mm. Mesh of the clamped part is shown in Figure 3.3.

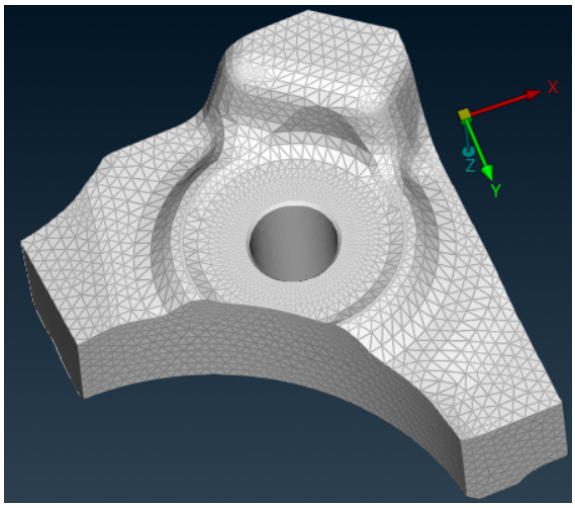

Figure 3.3: Clamped part: Mesh

A total of **78678** elements are created in the clamped part, of which 66962 are tetrahedral elements, and the remaining 11716 are the shell elements. The total number of nodes in the clamped part is **101204**.

3.1.1.3 Couplings and Springs

To constrain the translational and rotational movement of the bolt along x, y axes through the analysis, three springs are added on the top of the bolt in x, y, z directions and two springs are added on the bottom surface of the bolt in x, y directions. The stiffness of all these springs is 10 N/mm. The springs prevent any unwanted movement of the bolt due to uneven contact, while their low stiffness ensures that the bolt's actual rotation is not significantly affected by the springs.

Several couplings are created on the bolt and the clamped part for load application and result extraction. A kinematic coupling on the bolt head nodes is used to apply the torque on the bolt. In this study, it is important to calculate the rotational displacement of the bolt. Since the solid elements only have 3 degrees of freedom, it is not possible to extract the rotation about different axes directly from the nodal output. For this purpose, distributing couplings are introduced at several sections along the bolt. With the origin of the global coordinate system on the bolt axis under the bolt head, and z axis pointing towards the threads, the axial locations (z co-ordinates) of the distributing couplings along the bolt are given in Figure 3.5. These couplings are used to extract the displacement results at different sections as described in section 4.1.4. All the springs and couplings on the bolt are shown in Figure 3.4.

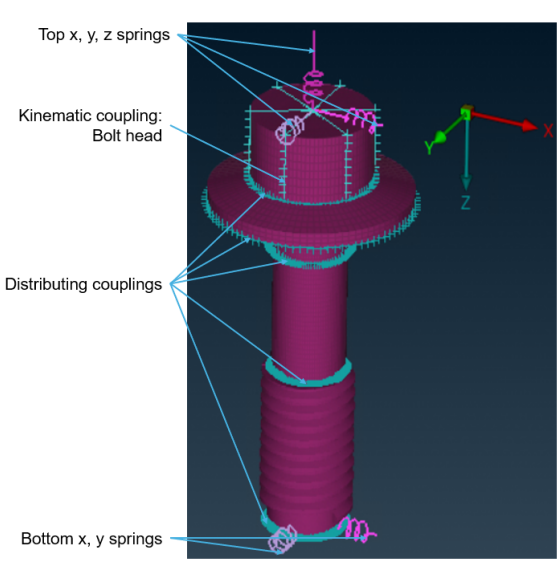

Figure 3.4: Springs on the bolt

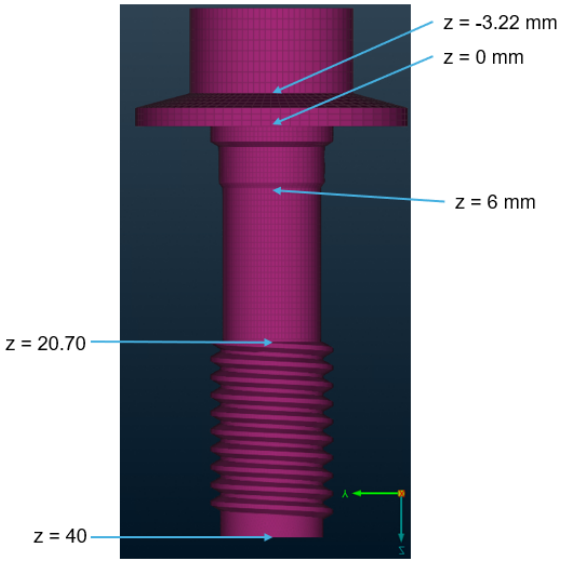

Figure 3.5: Distributing couplings defined at different sections on the bolt

Two distributing couplings are also introduced on the top and bottom surfaces of the clamped part with 4 nodes each. The radial distance of these nodes from the bolt axis is 7 and 9 mm respectively. The axial and rotational displacement is extracted at the reference nodes of these couplings. The nodes selected for these couplings are ≈ 90 deg. apart and at a radial distance of 7 mm and 9 mm from the bolt axis. The couplings are shown in figures 3.6 and 3.7.

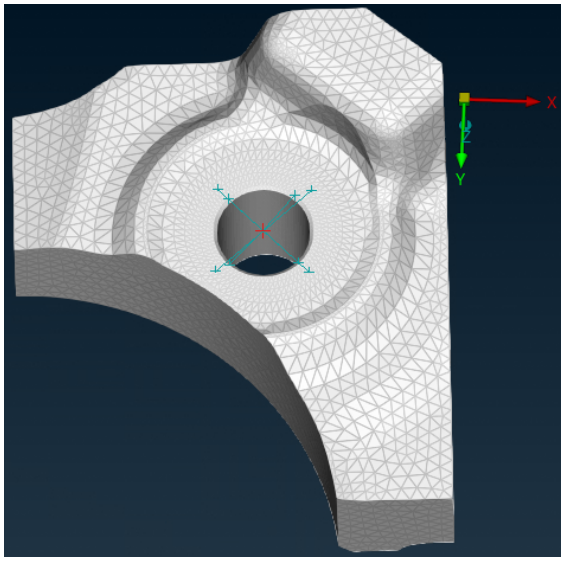

Figure 3.6: Clamped part - top surface couplings

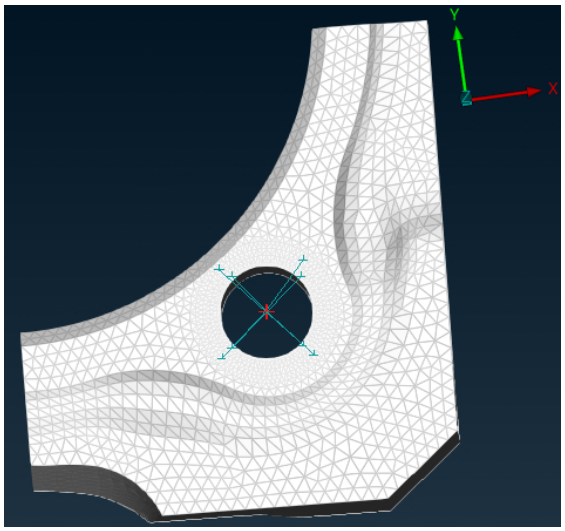

Figure 3.7: Clamped part - bottom surface couplings

3.1.2 Material

The bolt and the threaded part are made of steel, while the clamped part is made of aluminium. As described in Section 1.5 the analysis is run with linear elastic material models for all the parts. Material properties for the different parts are given in Table 3.5.

Table 3.5: Materials for different parts

Component	Material	Elastic Modulus [GPa]	Poisson's ratio
Bolt	Steel	207	0.3
Clamped Part	Aluminium	70	0.3
Threaded Part	Steel	207	0.3

3.1.3 Contact Conditions

Three different contact regions are present in the model, they are described in Table 3.6 and shown in Figure 3.8. Normal and tangential behaviours need to be defined for these contact surfaces.

Table 3.6: Different contact regions in the assembly

Interface	Main Surface	Secondary Surface
Bolt head - Clamped part	Bolt head	Clamped part
Clamped part - Threaded part	Threaded part	Clamped part
Internal and External threads	Internal threads (Threaded part)	External threads (Bolt)

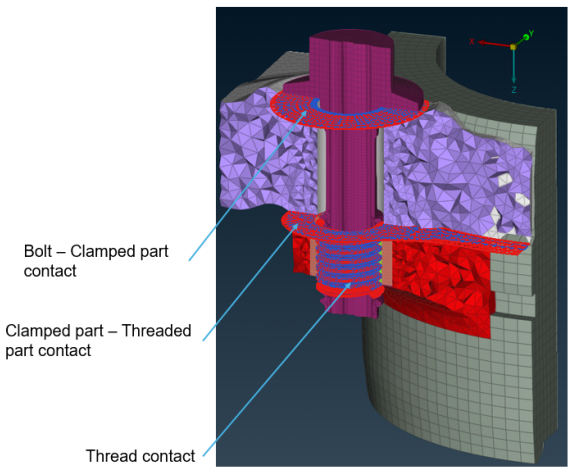

Figure 3.8: Different contact regions in the model

For the normal behaviour, "hard" pressure-overclosure relationship is applied with the Augmented Lagrange enforcement method for all contact definitions. The hard pressure - overclosure relationship enables the transmission of any pressure when

the clearance between the two contacting bodies is zero, and the pressure drops to zero as soon as the contact becomes open. In the Augmented Lagrange enforcement method, first the contact problem is solved through conventional penalty method, and then additional augmentation iterations are performed with Lagrange multipliers to get a new augmented pressure solution which eliminates any remaining penetrations [15]. The penalty method approximates "hard" pressure-overclosure behaviour through a linear relationship, whereby the transmitted force between the two bodies is proportional to the interference between the bodies [15]. Thus, small penetrations still may occur if the problem is solved by penalty method. In order to achieve a more accurate solution, Augmented Lagrange method is thus used.

The frictional behaviour between the contact surfaces depends on the underlying material behaviour, the contact pressure, and the lubrication conditions, as well as the relative sliding rate of the contact surfaces [3, 5, 6]. The variation in friction coefficients through the analysis is excluded in this study, as described in Section 1.5. Constant friction coefficient values based on the underlying materials of the contacting parts are shown in Table 3.7.

Table 3.7: Friction coefficients at different assembly interfaces

Interface	Materials	Coefficient of friction
Bolt head - Clamped part	Steel - Aluminium	0.18
Clamped part - Threaded part	Aluminium - Steel	0.18
Internal and External threads	Steel - Steel	0.12

3.1.4 Boundary Conditions

The motion of the nodes on the cylindrical surface of the bolt head is coupled with a node at the centre of the top surface of the bolt head through a kinematic coupling, as described in Section 3.1.1.3. This constraint is created to facilitate load application. Appropriate boundary conditions need to be applied to get a controlled motion of the bolt during the analysis. The boundary conditions are shown in figures 3.9 and 3.10. The boundary conditions described here are active throughout the analysis.

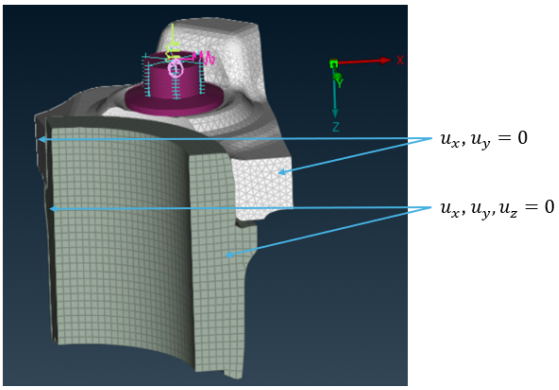

Figure 3.9: Boundary conditions on the clamped part and threaded part

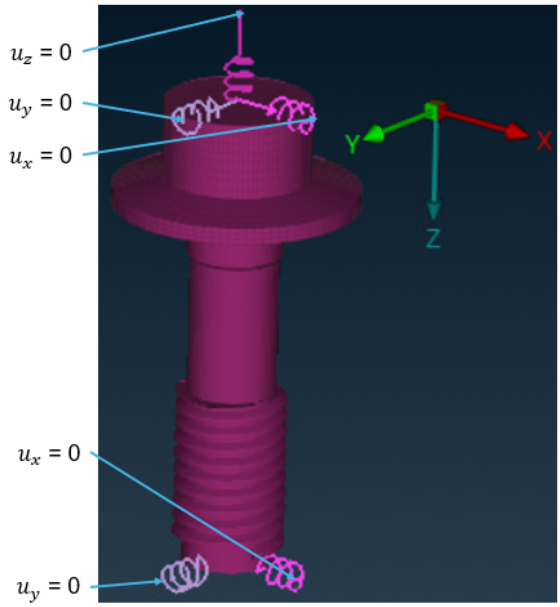

Figure 3.10: Boundary conditions on the bolt

- Fixed displacement in x and y directions on two surfaces of the clamped part that are parallel to the z axis. The translation degree of freedom for the clamped part along the z axis is kept free to simulate the actual conditions.
- Two surfaces on the threaded part, parallel to the z axis are constrained in x, y, z directions to prevent its rigid body motion.
- The nodes of the springs on the bolt are constrained along the direction of the spring axes.

3.1.5 Analysis Procedure

The nonlinear analysis consists of the following steps:

1. Contact initialisation
2. Torque application and removal

In the model, there are small gaps between contact surfaces. The gap between the thread surfaces is 0.01 mm. Between the bolt head and clamped part, there is a small gap of 0.01 mm, and between the clamped part and threaded part, there is a gap of 0.005 mm. The gaps are shown in Figure 3.11. The initial step closes the gaps and activate the contacts in the model between the threads and underneath the bolt head. The importance of this step is explained in Section 2.2. A rotational displacement of 0.037 rad (2.13 deg.) is applied on the kinematic coupling to close the gaps. Automatic contact stabilisation is also used in this step to avoid convergence problems.

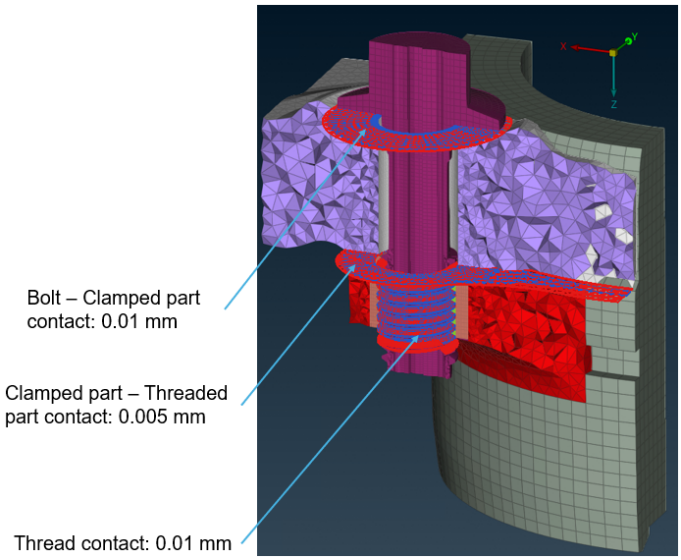

Figure 3.11: Gaps between the contact surfaces

The actual tightening process is simulated by applying a torque of 90 Nm on the bolt head. The torque is linearly increased to the target value of 90 Nm. To simulate tool removal (torque release), the torque is reduced back to 0 linearly in the same load step. This increase and decrease of the torque is defined with an amplitude curve. The automatic contact stabilisation from the contact initialisation step is disabled in this step to avoid its interference with the response for the model.

For both steps, a non-linear dynamic analysis is run with "quasi-static" application. Thus, in the first step of contact initialisation, the rotation is applied linearly by default. Additionally, discontinuous step control is also defined for both contact initialisation and torque application steps. All load steps in the analysis are summarised in table 3.8. The time period in the case of quasi-static conditions is only relevant for the load amplitude curve. The torque application curve is presented in Figure 3.13. The applied rotation in the contact initialisation step is plotted in Figure 3.12.

Table 3.8: Summary of analysis steps

Step	Type	Load / Boundary conditions	Step time
Contact initialisation	Non-linear dynamic - Quasi static	Rotation of 0.03729 rad. on the bolt head	0-1
Torque	Non-linear dynamic - Quasi static	Torque of 90 Nm on the bolt head	1-3

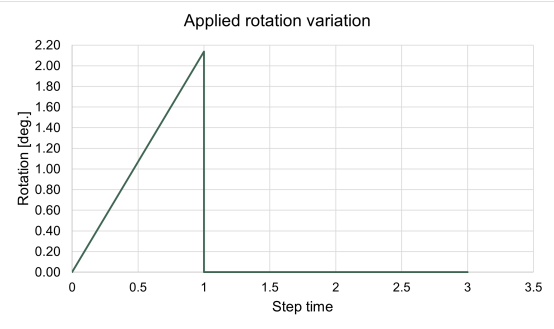

Figure 3.12: Rotation amplitude curve

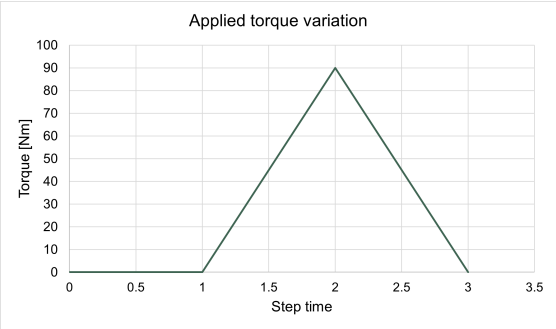

Figure 3.13: Torque amplitude curve

Results at three points are important for this analysis - after the contact initialisation step (at step time 1), at full torque application (90 Nm, step time 2), and after torque release (step time 3).

3.2 Hand Calculations

In this section, the hand calculation procedure followed to calculate the generated preload and different friction torque components is given.

To get benchmark values for the FE results torques at different sections of the joint were calculated with the following steps: The values of under-head and thread frictional torques, as well as the preload are estimated with the long form torque-preload equations [2]. Some deviation is expected between the hand calculation and the analysis results, as several stress concentration factors are not taken into account for the hand calculations. The procedure for hand calculations is based on the 'long form equation' for torque - preload relationship given in [2] and is described below. The data used for hand calculations as well as the finite element analysis is given in Table 3.9.

Table 3.9: Baseline model - hand calculation data

Parameter	Value
Applied torque ($T_{applied}$) [Nm]	90
Under-head friction coefficient ($\mu_{underhead}$)	0.18
Thread friction coefficient (μ_{thread})	0.12
Diameter of the bolt hole (d_h) [mm]	14
Diameter of the bolt flange (d_w) [mm]	26.6
Equivalent friction diameter of the threads (d_m) [mm]	10.863
Thread pitch (p) [mm]	1.75

1. Calculate equivalent friction diameter of the under-head contact surface:

$$D_{km} = \frac{d_h + d_w}{2} \tag{3.1}$$

D_{km} is the equivalent friction diameter of the under-head contact surface. In this case: The diameter of the bolt hole is 13 mm. However, effective contact region starts at a diameter of 14 mm due to a chamfer on the clamped part near the bolt hole. Thus, it is taken as the diameter of the bolt hole.

2. Calculate preload force from the applied torque with the following equation:

$$T_{applied} = F_{preload}\,(\mu_{underhead}\,\frac{D_{km}}{2} + 0.578\,\mu_{thread}\,d_m + 0.159\,p) \tag{3.2}$$

Here, $F_{preload}$ is the generated preload.

3. Calculate thread friction torque, under-head friction torque, and pitch torque with the following equations:

$$T_{thread} = 0.578\,\mu_{thread}\,F_{preload}\,d_m \tag{3.3}$$

$$T_{underhead} = \mu_{underhead}\,F_{preload}\,\frac{D_{km}}{2} \tag{3.4}$$

$$T_{pitch} = F_{preload}\frac{p}{2\,\pi} = 0.159\,p\,F_{preload} \tag{3.5}$$

4. Calculate the shank torque from the applied torque and under-head friction torque as:

$$T_{shank} = T_{applied} - T_{underhead} \tag{3.6}$$

3.3 Under-head Friction Variation

In the baseline model the under-head friction torque is 63.9% of the applied torque, as can be seen in Table 3.10, based on hand calculation results. In this case, the bolt head is not expected to slip back with torque release as the shank torque is significantly lower than the under-head friction torque, as described in Section 2.2.1. The same behaviour is seen in the baseline analysis results. Three additional values of the under-head friction coefficient are tested, keeping the thread friction coefficient the same as in the baseline analysis, i.e. 0.12. The values of the friction coefficient tested are determined through hand calculations, where three cases are considered. They are as follows: First where shank torque is 55% of the applied torque, second where shank torque is 45% of the applied torque, and third where the shank torque is 60% of the applied torque. The required value of $\mu_{underhead}$, and the corresponding $F_{preload}$ value is calculated by rearranging the equations from section 3.2 as follows:

$$T_{shank} = \alpha\,T_{applied} \tag{3.7}$$

$$T_{underhead} = (1-\alpha)\,T_{applied} \tag{3.8}$$

$$\therefore \alpha\,T_{applied} = F_{preload}(0.578\,\mu_{thread}\,d_m + 0.159\,p) \tag{3.9}$$

$$(1-\alpha)\,T_{applied} = \mu_{underheadd}\,F_{preload}\,\frac{D_{km}}{2} \tag{3.10}$$

Here, α is the ratio of the shank torque w.r.t the applied torque value, which is set according to the case. The preload force and under-head friction coefficient are determined through equations 3.7 - 3.10. The thread friction torque and pitch torque

are calculated with the obtained $F_{preload}$ value from equation 3.9 according to equations 3.3 and 3.5 respectively.

Table 3.10: Hand calculation results for different under-head friction coefficients tested

	α	$\mu_{underhead}$	$T_{underhead}$	T_{shank}	T_{thread}	T_{pitch}	$F_{preload}$
Baseline	-	**0.18**	**57.5**	**32.5**	**23.7**	**8.8**	**31482.5**
Case 1	0.45	0.12	49.5	40.5	29.6	10.9	39255.3
Case 2	0.55	0.08	40.5	49.5	36.1	13.4	47978.7
Case 3	0.6	0.07	36	54	39.4	14.6	52340.1

Even though the underlying materials for both bolt-clamped part interface, and clamped part-threaded part interface are the same and thus realistically the friction coefficients at these interfaces should also be the same, while varying the under-head friction, the friction coefficient between the clamped part and the threaded part is kept the same as in the baseline model, i.e. 0.18. This is done to isolate the effect of friction at the bolt - clamped part interface. The values of the friction coefficients tested, the shank torque, under-head friction torque, thread torque and preload force results from hand calculations for these three cases are given in Table 3.10.

4

Results

The results from both baseline analysis, and friction variation study are presented in this chapter. For the baseline analysis, results of contact pressures, axial and torsional displacements, torque and preload evolution, as well as stresses in the joint components are presented. For the friction variation study, results are presented in terms of the variation in bolt preload, shank torque, and twist in the shank during torque removal process. Additionally, variation in torque components throughout the analysis for different conditions of under-head friction is shown. Finally, the modelling choices that may have affected the results are described.

4.1 Baseline model

4.1.1 Bolt - Clamped part Contact

The average contact pressure on the top surface of the clamped part is plotted against the radial distance from the bolt axis, at full torque level in Figure 4.2. This is calculated by taking the average of contact pressures of nodes at different radial distances from the bolt axis. The radial distances of nodes on the thread surfaces are shown in figure 4.5. The actual contact pressure distribution at step time 2 is shown in Figure 4.1. There is a significant pressure difference between the inner and the outer edge, however 85% of the total pressure reduction occurs close to the inner edge itself. It is also found that the average contact pressure at the inner and outer edge increase by 0.04% and 2.1% respectively when the torque is reduced back to 0, however, a small pressure drop ($< 0.5\%$) is seen for all the intermediate nodes.

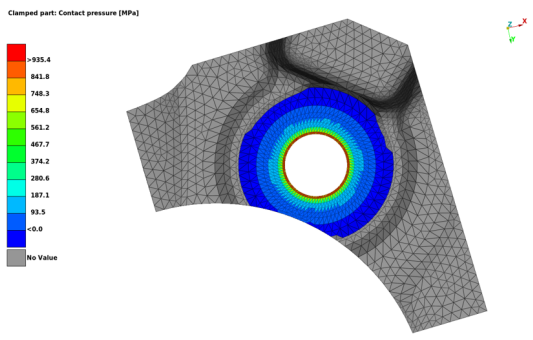

Figure 4.1: Under-head contact pressure distribution at 90 Nm

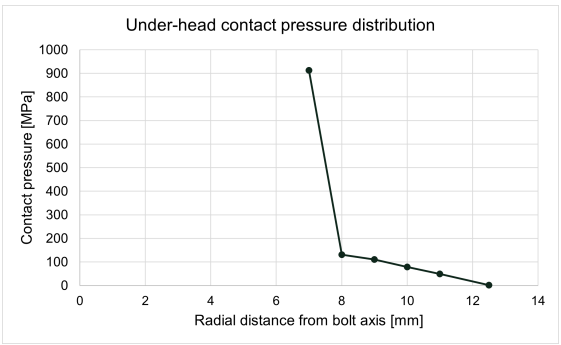

Figure 4.2: Average under-head contact pressure at 90 Nm

4.1.2 Thread Contact

In the model, there are ≈ 5.5 threads that have active contact. The contact pressure decreases from the tip to the root of the thread on the bolt. A significant increase is seen for the nodes on the edge of the root of the thread. The thread numbers are shown in Figure 4.3. On every thread, there are 5 nodes along the radial direction, as shown in Figure 4.5. Contact pressures on the nodes at the same radial distance from the bolt axis are averaged and plotted for the first 5 engages threads in Figure 4.6.

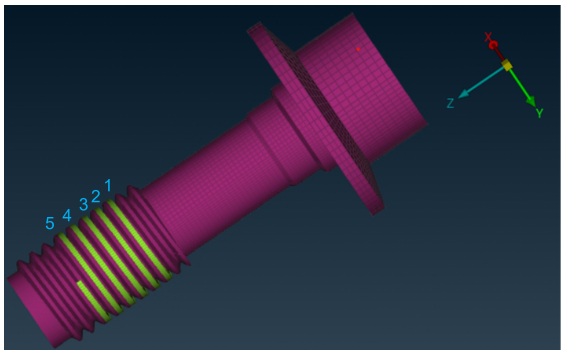

Figure 4.3: Bolt thread numbers

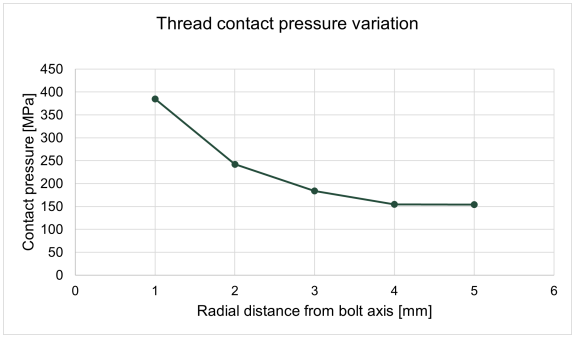

Figure 4.4: Variation in contact pressure at different points along the bolt at 90 Nm

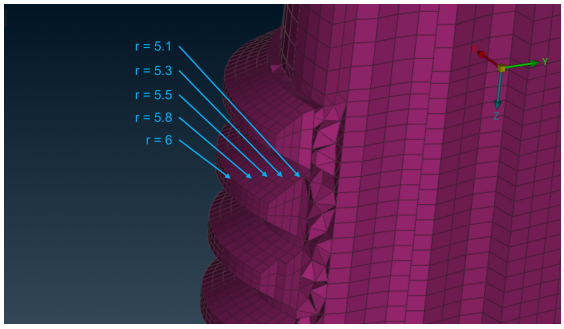

Figure 4.5: Radial locations of nodes on the thread surface

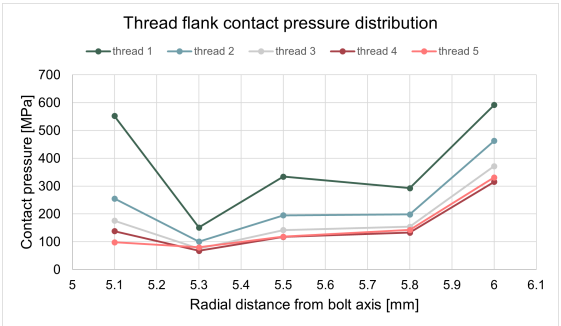

Figure 4.6: Average contact pressure at different threads at 90 Nm

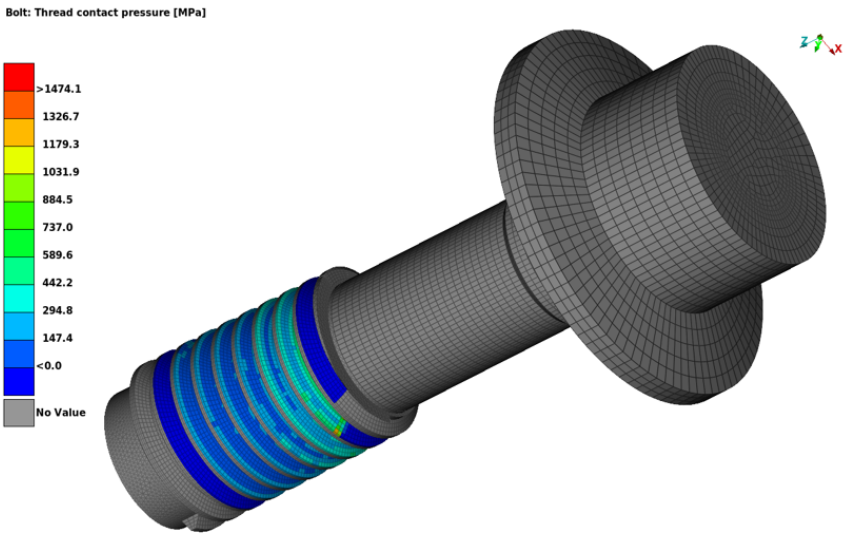

Figure 4.7: Contact pressure distribution at 90 Nm

The variation of average thread contact pressure at different threads is shown in Figure 4.4. Average contact pressure for each thread is calculated by taking the average of contact pressure result for all nodes in that thread. Contact pressure decreases from the first to the fourth engaged thread, and remains the same for the fifth engaged thread. The pressure drop from the first to the fifth thread is $\approx 60\%$. Thread contact pressure distribution is shown in Figure 4.7.

4.1.3 Clamped part - Threaded part Contact

Contact between clamped part and threaded part is defined in two parts due to different element orders on the surface of the threaded part. The different surfaces are shown in Figure 4.8. This causes pressure concentration at the boundary nodes, which is unrealistic, as can be seen in Figure 4.9. The contact pressure is high near the bolt hole at this interface as well, however, the pressure is almost zero at a distance from the bolt hole. The contact pressure distribution is shown in Figure 4.9.

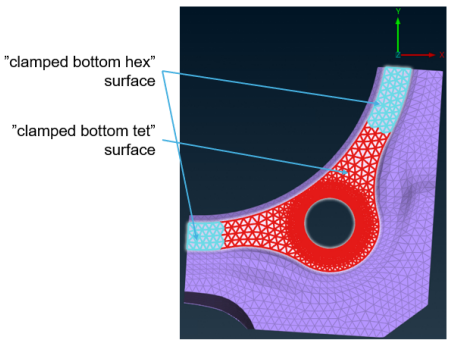

Figure 4.8: Different contact surfaces at the clamped part - threaded part contact interface

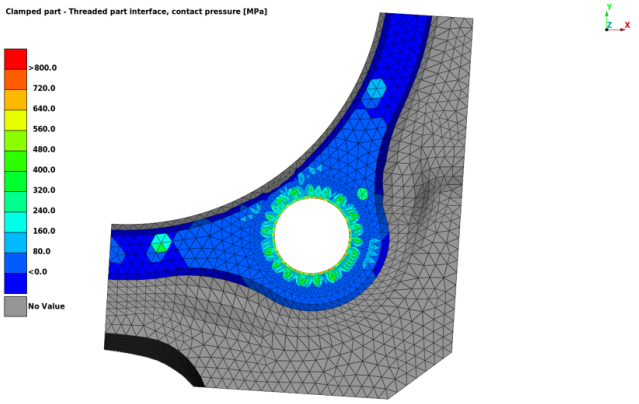

Figure 4.9: Contact pressure distribution at the clamped part - threaded part interface

4.1.4 Axial and Torsional Displacement Results

Figures 4.11 and 4.12 show the relative axial and rotational displacements between four points as described in Figure 4.10. These points are the reference nodes of the couplings at these sections, described in Figure 3.5. The axial and rotational displacement is extracted and the relative values of displacements are plotted through torque application (step time 1-2) and torque removal (step time 2-3).

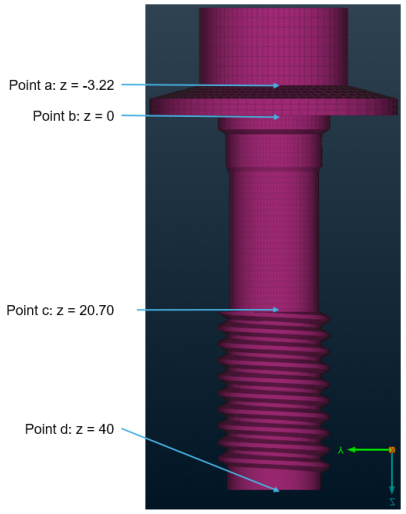

Figure 4.10: Points at different sections of the bolt

From the plot of relative axial displacement in Figure 4.11, it can be concluded that the maximum deformation is in the bolt shank, indicated by the gap in the curves of points c and b. When the applied torque is reduced back to zero, the axial deformation in the bolt remains almost constant.

Figure 4.11: Relative axial displacement of points at different sections along the bolt axis

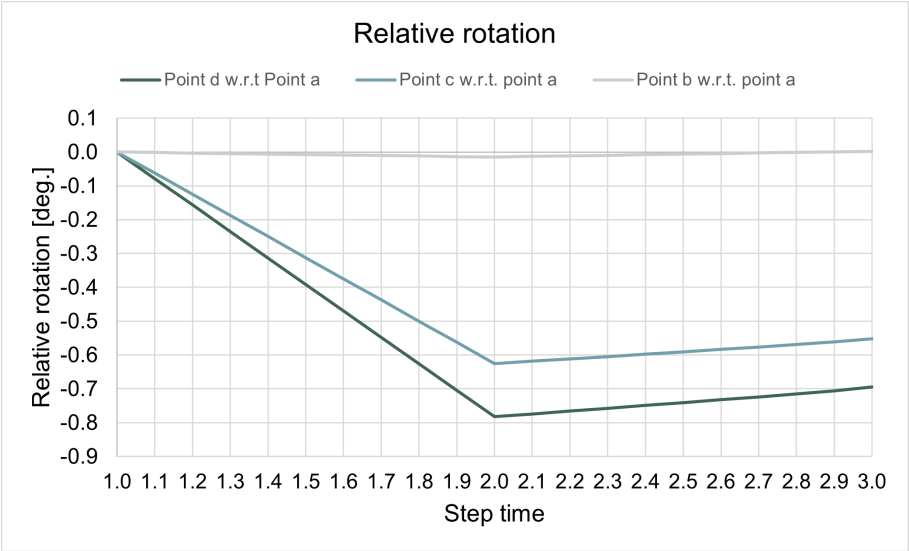

Figure 4.12: Relative rotational displacement of points at different sections along the bolt axis

The relative rotational displacement plot in Figure 4.12 also indicates that most of the bolt twist is present in the bolt shank. The stretch and twist in the threaded part of the bolt is significantly lesser than the shank. When the torque is released, the magnitude of the rotational deformation decreases due to linear elastic material behaviour.

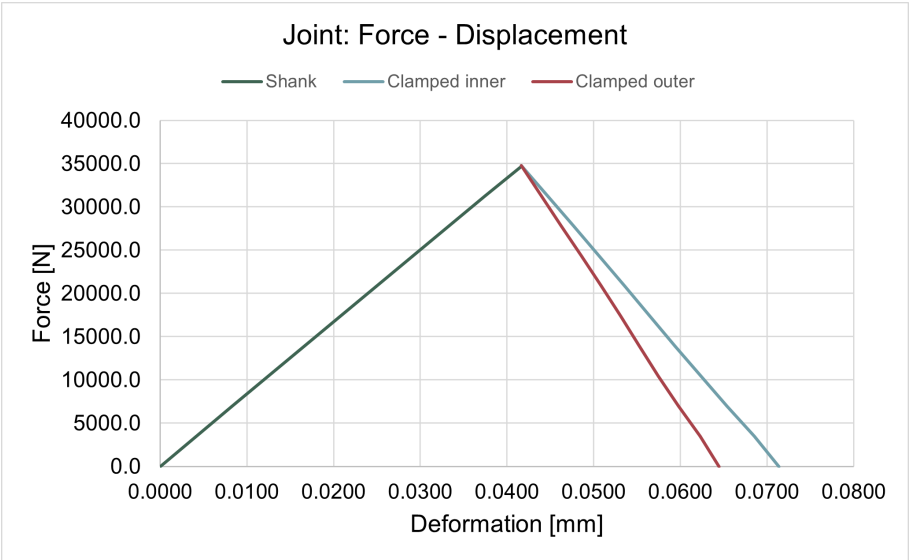

Figure 4.13: Axial force and deformation in the bolt and the clamped part

Figure 4.13 shows the force-displacement plot for the joint, i.e. the bolt shank and the clamped part, where the stretch and preload force in the bolt shank is plotted with the compression and clamping force on the clamped part. The deformation in the clamped part is measured at two radial locations as described in Section

3.1.1.3. The curve "clamped inner" in Figure 4.13 represents the deformation at a radial distance of 7 mm from the axis, while the curve "clamped outer" represents the deformation of points 9 mm away from the bolt axis. The inner edge of the clamped part is expected to be compressed more than the outer edge. The bolt shank stretches by 0.04 mm, while the clamped part is compressed by 0.03 mm. This gives a stiffness of 8.34 $\times 10^5$ N/mm for the shank of the bolt. Considering the length L, elastic modulus E and cross sectional area A of the shank, the stiffness of the shank calculated as $K = \frac{E\,A}{L}$ is 7.7 $\times 10^5$ N/mm. The difference in compression between the inner and outer points on the clamped part is ≈ 0.007 mm.

4.1.5 Torque Evolution Through Time

Figure 4.14 shows the variation of different torque components through time.

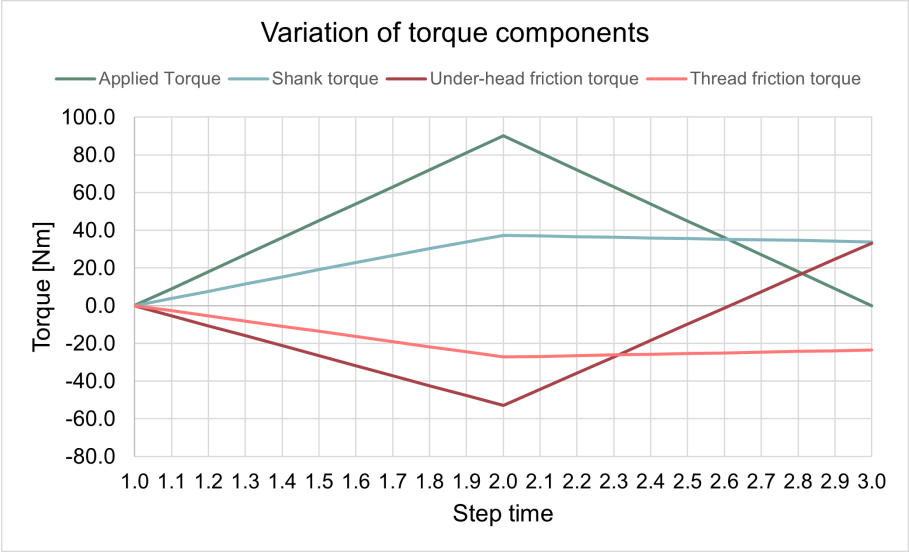

Figure 4.14: Variation of different torque components through the analysis

With linear increase of the torque applied on the bolt head, all the frictional components increase linearly. The differences between the values of frictional torque components predicted by the hand calculations and the FE results are expected due to the following causes:

- The hand calculations assume constant contact pressure under the bolt head and the thus the equivalent friction radius to be the average of the shank and flange radius of the bolt. However, the contact pressure at the inner edge is significantly more than the outer edge, which reduces the effective under-head friction radius.

- There are several stress concentration factors that are omitted in the hand calculations.

When the torque is reduced from 90 Nm to simulate the condition after removal of torque wrench, the shank torque reduces at a much slower rate, as the all the contact surfaces resist the reverse motion of the bolt through friction. When the torque is released completely, the shank torque value is reduced to 33.1 Nm, 6 mm away from the bottom of the bolt head. The torques induced by the frictional forces at the bolt-clamped interface, as well as the threads interface also increase linearly during torque application process (step time 1 to 2), and decrease at a lower rate during torque release (step time 2 to 3). After the torque is completely released, there is equilibrium between the shank torque and the torque induced by the frictional forces at the bolt-clamped part interface.

4.1.6 Preload Evolution Through Time

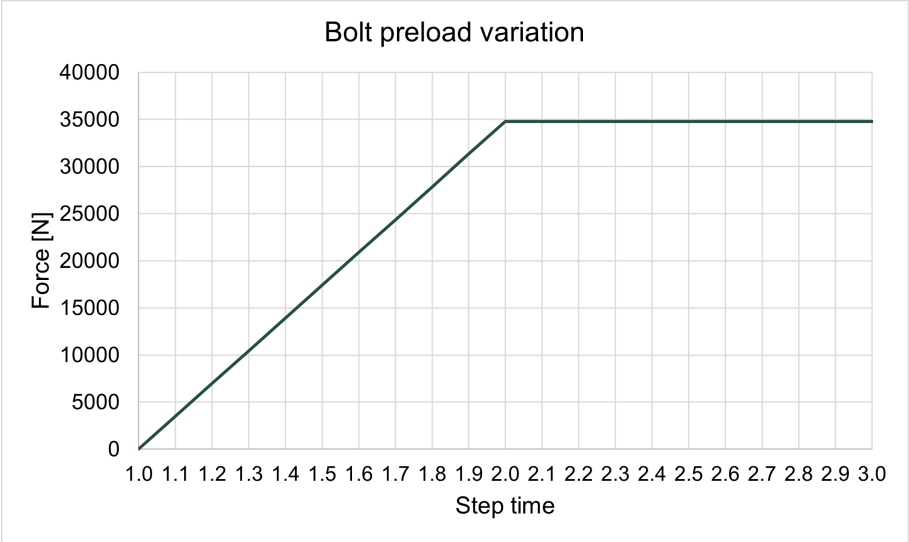

Figure 4.15: Bolt preload variation through analysis

Figure 4.15 shows the change in bolt preload during application and removal of the torque. The preload increases linearly with time. During torque release process, the preload drops by 0.067 %. This reduction in preload is only caused by the reduction in the torsion of the joint elastically.

4.1.7 Agreement between Hand Calculation and FE Results

Overall, the results from the baseline model are in agreement with the hand calculations in terms of equilibrium of forces and moments. However, the individual contributions of different torque components show some variation, resulting in a variation in the generated preload value as well. The under-head friction torque is found to be lesser than the value obtained from hand calculations, while the thread and pitch torque components are found to have higher values than the calculated estimates. However, it can be noted that the ratio of T_{thread} to T_{shank} is almost the same in both the hand calculations and the FE results. This indicates that the discrepancy between the torque results in the FE analysis and the hand calculations

can be attributed to the error in calculation of the under-head equivalent friction radius. The FE and hand calculation results are given in Table 4.1.

Table 4.1: Comparison of hand calculation and FE results

Torque component	Hand calculation (90 Nm applied torque)	FE results at 90 Nm applied torque
$T_{underhead}$[Nm]	57.5	53.0
T_{shank}[Nm]	32.5	36.5
T_{thread}[Nm]	23.7	27.3
T_{pitch}[Nm]	8.8	9.7
$F_{preload}$[N]	31482.8	34804.2

4.1.8 Equivalent Stress Results

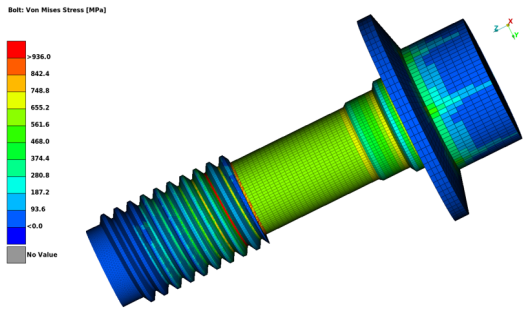

Figure 4.16: Bolt: Von Mises stress

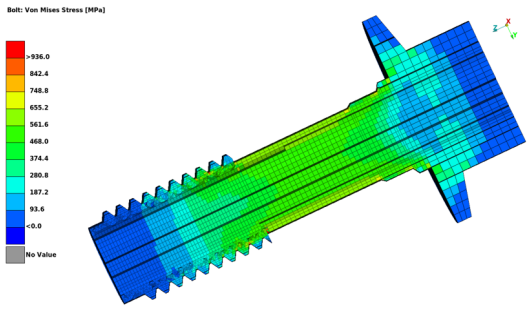

Figure 4.17: Bolt: Von Mises stress - section view

Yield strength of the bolt is 936 MPa. The bolt has maximum stress at the root of the first thread. The von Mises stress distribution in the bolt is plotted in figures 4.16 and 4.17. The stress level is significantly below the yield strength in the bolt of the bolt. The von Mises stress reduces from the first to the last engaged thread as the load carried by the thread decreases. In the bolt flange, the stress is minimum at the outer edge as the contact pressure is also minimum at that location. Stress concentration is also seen at the sections where the diameter of the shank changes, as well as at the interface of two different mesh regions.

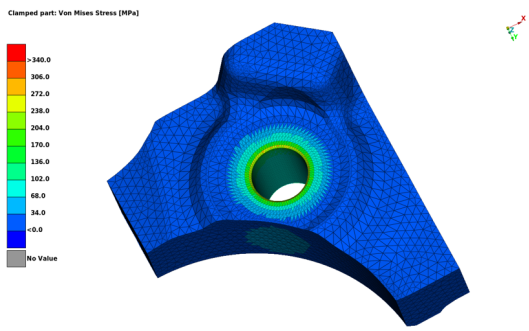

Figure 4.18: Clamped part: Von Mises stress - from top

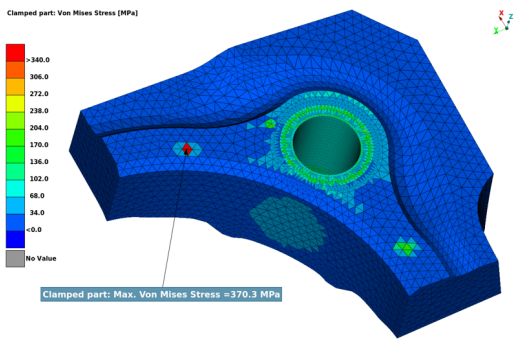

Figure 4.19: Clamped part: Von Mises stress - from bottom

The clamped part has a yield strength of 340 MPa. Stresses generated in the clamped part are also well within the elasticity limit, and only two elements are found to have von Mises stress above yield strength. However, this can be regarded as an anomaly as these elements lie on the boundary between two contact regions, which has interfered with the results. The stress distribution in the clamped part is presented in figures 4.18 and 4.19.

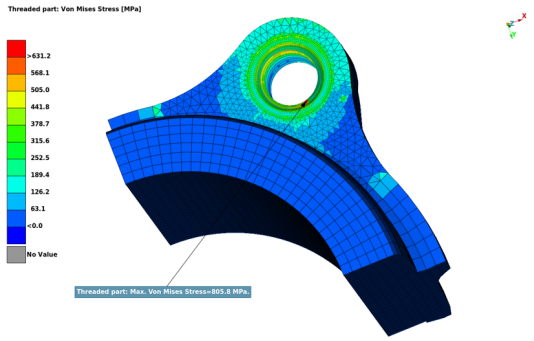

Figure 4.20: Threaded part: Von Mises stress - from top

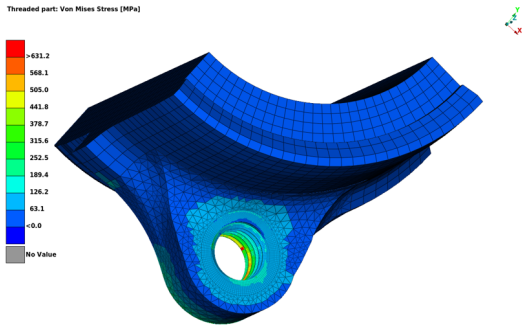

Figure 4.21: Threaded part: Von Mises stress - from bottom

Yield strength of the threaded part is 631.2 MPa, and the von Mises stresses in the threaded part are significantly below the elastic limit. The highest stresses are present in the threads, and the magnitude of the stress drops from he first to the last engaged thread. The threaded part von Mises stresses are shown in figures 4.20 and 4.21.

4.2 Effect of Under-head Friction

From the baseline model, it can be seen that the drop in the shank torque and force is very small under torque removal under the given friction conditions. The analysis was run with different values of $\mu_{underhead}$ to see its effect on the tightening and loosening behaviour. The results are presented in terms of variation of shank force, shank torque, shank rotational deformation w.r.t the friction coefficient. Additionally, the variation of different torque components through the analysis is also shown for different cases of under-head friction coefficient.

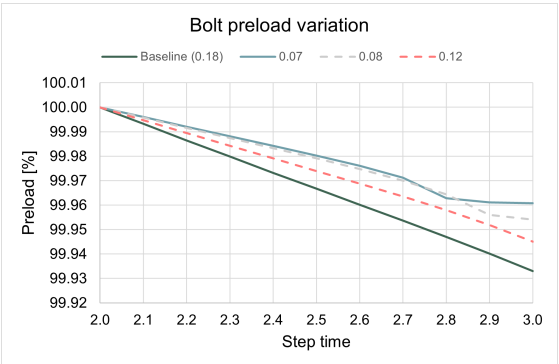

Figure 4.22: Preload drop

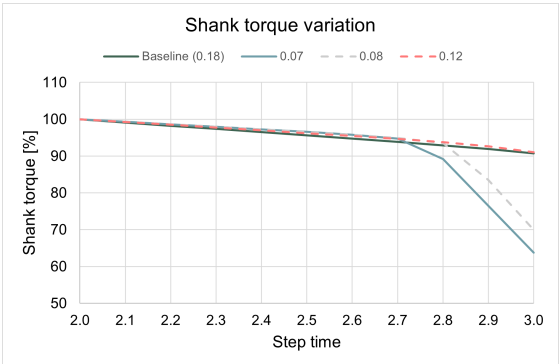

Figure 4.23: Shank torque drop

Figures 4.22-4.24 show the drop in preload, shank torque and shank twist for different values of $\mu_{underhead}$ during torque removal process, i.e. from step time 2 to 3. Running time for the analysis is also seen to drop if the under-head friction coefficient is lowered.

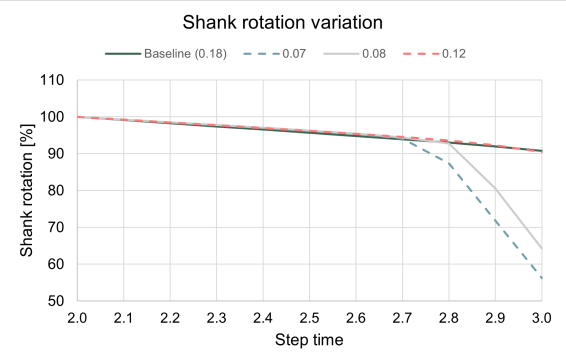

Figure 4.24: Reduction in twist of the bolt shank

With elastic spring-back only, the rate of loss of preload, shank torque and shank twist remains constant, as can be seen for the plots of $\mu_{underhead} = 0.18$ and $\mu_{underhead} = 0.12$ in figures 4.22 - 4.24. With reduction in the friction coefficient value, the threshold for slip decreases, the shank torque drops at a higher rate. The back rotation also increases after slip. While the shank torque and rotation reduce considerably during torque removal, the preload value does not drop significantly.

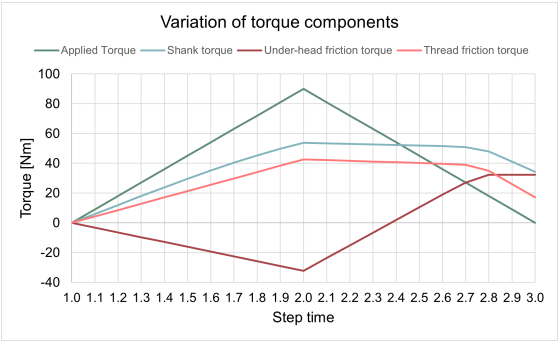

Figure 4.25: Case 1: $\mu_{underhead} = 0.07$

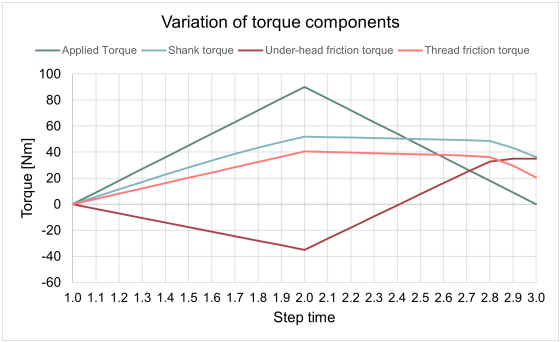

Figure 4.26: Case 2: $\mu_{underhead} = 0.08$

Figures 4.25, 4.26 and 4.27 show the variation in different torque components over time for different friction coefficients. Figures 4.25, 4.26 show the slip at the under-head contact interface. With reduced friction coefficient, the under-head slip starts at a higher value of applied torque during the torque removal process. With $\mu_{underhead} = 0.12$, there is no slip under the bolt head.

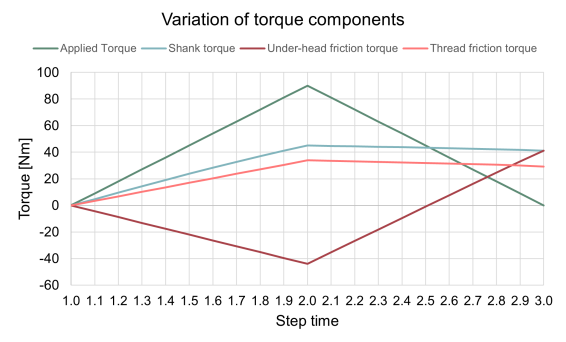

Figure 4.27: Case 3: $\mu_{underhead} = 0.12$

4.3 Sources of Error

While the methods selected to complete this project provide a good balance between simplicity and accuracy, certain modelling choices may have affected the results. They are as follows:

- The material model used for all the components in this analysis is linear elastic. Von Mises stresses are found to be exceeding the yield strength of the bolt at the root of the first engaged thread in the baseline analysis. While the higher stresses are not spread inside, defining a plastic material behaviour can still affect the results.

- There are different ways to achieve contact initialisation, which affect the force, contact pressure and torque results. Applying a small rotation results in torque generated in the bolt. A small shank force (21.06 N) is also generated in the bolt in the contact initialisation step itself. The effect of this would have been more important to consider had plastic behaviour been considered in the analysis, however, the results are also affected even if the material behaviour is linear elastic.

5

Conclusion

In this project, the behaviour of a bolted joint during its tightening process was studied with a 3D finite element analysis. A torque of 90 Nm was applied and then removed on a M12 $\times$ 1.75 mm bolt, and the resulting rotation of the bolt, along with change in frictional torque components at the assembly interfaces was studied. The relationship between applied torque and the preload generated in a bolt was obtained through finite element analysis, which has been found to be agreeing reasonably well with the analytical formulations. The effect of changing the under-head friction coefficient on the torque and preload drop in the bolt shank was established both quantitatively and qualitatively. From the study, the following conclusions can be drawn:

- The preload generated in the bolt varies linearly with applied torque during tightening. This agrees well with the hand calculations.

- The hand calculations and finite element results show 10.6 % deviation in terms of the preload generated in the bolt. The finite element results indicate that the under-head friction torque is over- estimated in the hand calculations.

- The frictional torque components, as well as the preload increase linearly when the applied torque torque on the bolt is linearly increased .

- The finite element results give similar stiffness for the bolt shank as hand calculation with the formula $K = \frac{EA}{L}$, considering the bolt shank as cylinder of varying diameter.

- Magnitude of preload drop due to elastic spring back as well as slip under the bolt head is not significant ($< 0.07\%$).

- When there is no slip at the under-head contact interface, i.e. under elastic spring-back only, the preload drop is linear and under-head slip induces non-linearity in the preload loss.

- Under-head slip causes the preload to stabilise but accelerates the drop of shank torque and shank twist.

- Lower value of $\mu_{underhead}$ causes slip earlier during torque removal procedure, i.e., at a higher value of shank torque.

5.1 Scope for future work

In this study, the tightening process of a bolted joint was studied under torque control with linear elastic material models. While the FE analysis predicts the generated preload in the bolt in reasonable agreement with the hand calculations and experimental data, there is room for improvement in terms of efficiency of the analysis.

In this study, a dynamic step was used with quasi-static application in ABAQUS to avoid convergence issues with unconstrained rigid body motion in the clamped part. However, the analysis can converge quicker with a non-linear static step. Further, choice of contact initialisation step would also affect the speed of the analysis. A static step without any loads can be tested for contact initialisation, which could possibly eliminate the requirement of contact stabilisation as well.

When the torque wrench is removed in reality, the change in torque applied on the bolt is instantaneous. While it is difficult to simulate that in FE analysis, different loading curves for torque removal can be tested to analyse their effect on the response.

Embedding is commonly observed in bolted joints, where the surface roughness at the bearing surface undergoes plastic deformation during torque application. This would not only change the frictional properties of the interface in reality, but also the resulting preload force. Introducing plastic material behaviour to simulate plastic deformation of the bearing surface, would improve the accuracy of the results.

The under-head contact area affects the clamping force exerted on the clamped part. Simulating the model with different flange areas for the bolt would help to identify its effect on the stiffness of the joint.

In this study, the relative motion of nodes at the contact interfaces is governed by the material elasticity, and friction. Introducing plastic material behaviour for the bolt would help determine the effect of thread plastic deformation on the torque release process, as it would affect the twist in the threaded part of the bolt, and subsequently, loosening behaviour.

Finally, The model can also be used to analyse the assembled joint's response under external loads. Incorporating actual variation in preload after assembly would make the analysis of an assembly more realistic, and accurate.

Bibliography

[1] Toshio Hattori and Tomohiro Naruse. *Solid Mechanics and Its Applications Compendium for Design and Manufacturing of Bolted Joints Mechanical Design Handbook for Failure Prevention of Products*. Tech. rep.

[2] John H Bickford and Michael Oliver. *Introduction to the Design and Behavior of Bolted Joints: Non-Gasketed Joints: Fifth Edition*. Tech. rep.

[3] Sayed A. Nassar, G. C. Barber, and Dajun Zuo. "Bearing friction torque in bolted joints". In: *Tribology Transactions* 48.1 (Jan. 2005), pp. 69–75. ISSN: 10402004. DOI: 10.1080/05698190590899967.

[4] Linbo Zhu, Jun Hong, and Xiangjun Jiang. "On controlling preload and estimating anti-loosening performance in threaded fasteners based on accurate contact modeling". In: *Tribology International* 95 (Mar. 2016), pp. 181–191. ISSN: 0301679X. DOI: 10.1016/j.triboint.2015.11.006.

[5] Kaiwen Guo, Tinglian Zhang, and Huang Yuan. "Experimental and computational investigations of nonlinear frictional behavior in threaded fasteners". In: *Tribology International* 154 (Feb. 2021). ISSN: 0301679X. DOI: 10.1016/j.triboint.2020.106737.

[6] Sayed A. Nassar, Payam H. Matin, and Gary C. Barber. "Thread friction torque in bolted joints". In: *Journal of Pressure Vessel Technology, Transactions of the ASME* 127.4 (Nov. 2005), pp. 387–393. ISSN: 00949930. DOI: 10.1115/1.2042474.

[7] Mingpo Zheng et al. "Initial losing behavior of pre-tightening force for threaded fastener during repeated tightening". In: *Engineering Failure Analysis* 134 (Apr. 2022). ISSN: 13506307. DOI: 10.1016/j.engfailanal.2021.106021.

[8] *T. Fukuoka Finite Element Simulation of Tightening Process of Bolted Joint With a Tensioner*. Tech. rep. 1992. URL: http://asmedigitalcollection.asme.org/pressurevesseltech/article-pdf/114/4/433/5623298/433_1.pdf.

[9] Toshimichi Fukuoka and Tomohiro Takaki. "Elastic Plastic Finite Element Analysis of Bolted Joint during Tightening Process". In: *Journal of Mechanical Design* 125.4 (2003), pp. 823–830. ISSN: 10500472. DOI: 10.1115/1.1631579.

[10] D G Sopwith and M I E Mech. *The Distribution of Load in Screw Threads*. Tech. rep.

[11] Qingmin Yu, Honglei Zhou, and Libin Wang. "Finite element analysis of relationship between tightening torque and initial load of bolted connections". In: *Advances in Mechanical Engineering* 7.5 (May 2015), pp. 1–8. ISSN: 16878140. DOI: 10.1177/1687814015588477.

[12] Zhifeng Liu et al. “Analysis of self-loosening behavior of high strength bolts based on accurate thread modeling”. In: *Engineering Failure Analysis* 127 (Sept. 2021). ISSN: 13506307. DOI: 10.1016/j.engfailanal.2021.105541.

[13] D. P. Hess. “Effect of Component Twist on Friction in a Bolted Joint”. In: *Journal of Failure Analysis and Prevention* 21.2 (Apr. 2021), pp. 669–677. ISSN: 18641245. DOI: 10.1007/s11668-020-01112-4.

[14] C. J. Dyson et al. “Tribological considerations of threaded fastener friction and the importance of lubrication”. In: *Tribology International* 191 (Mar. 2024). ISSN: 0301679X. DOI: 10.1016/j.triboint.2023.109162.

[15] *Abaqus - User Assistance R2026x*. URL: https://help.3ds.com/HelpDS.aspx?P=DSDoc&L=English&contextscope=cloud&F=FrontmatterMap/DSDoc-r-Abaqus.htm.

DEPARTMENT OF SOME SUBJECT OR TECHNOLOGY
CHALMERS UNIVERSITY OF TECHNOLOGY
Gothenburg, Sweden
www.chalmers.se

CHALMERS
UNIVERSITY OF TECHNOLOGY